CHALMERS

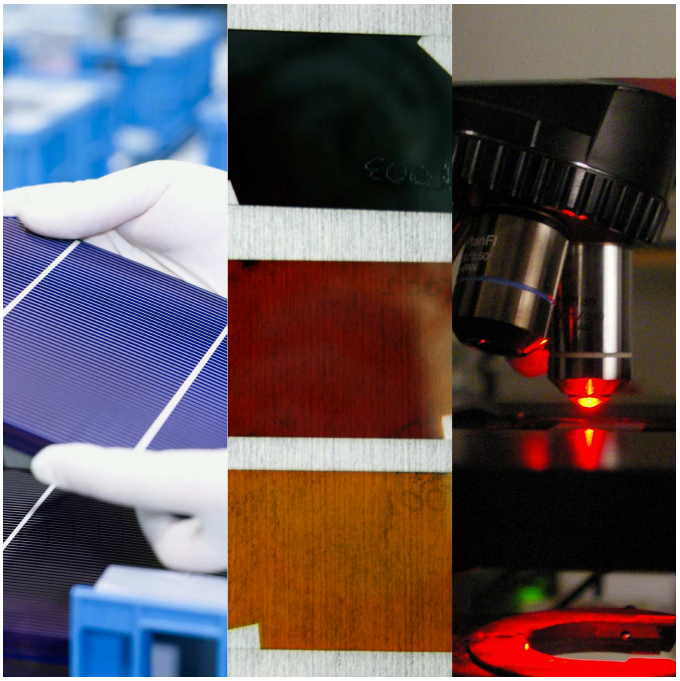

Fabrication and characterization of Mg-Ni hydride thin films for photovoltaic applications

Master of Science Thesis in the Master Degree Programme, Applied Physics

SIMON LINDBERG

Department of Applied Physics
CHALMERS UNIVERSITY OF TECHNOLOGY
Gothenburg, Sweden 2013

Fabrication and characterization of Mg-Ni hydride thin films for photovoltaic applications
SIMON LINDBERG

Cover: To the left is an image of a mono crystalline silicon solar cell [27], In the middle is an image of three samples of $Mg_{2.4}NiH_4$ annealed at different temperatures and to the right is a picture taken of the Raman equipment used in the thesis.

Department of Applied Physics
Chalmers University of Technology
SE-412 96 Gothenburg, Sweden

Fabrication and characterization of Mg-Ni hydride thin films for photovoltaic applications

Master of Science Thesis conducted in collaboration with Institute for Energy Technology, Lillestrøm.

SIMON LINDBERG
Department of Applied Physics
Chalmers University of Technology

Abstract

We prepared and characterized three different compositions of the novel semiconductor material $Mg_{2.0}NiH_4$, $Mg_{2.2}NiH_4$ and $Mg_{2.4}NiH_4$ as thin films for photovoltaic applications.

The thin films were deposited using reactive sputtering at room temperature, to achieve crystallization the samples were annealed at 220C and 290C. The composition of the samples were determined with EDS and the structural properties of the samples were then investigated using XRD and Raman spectroscopy. The band gap for the different compositions and annealing processes were calculated using a Tauc-plot.

We did Hall-measurements to investigate the electronic properties such as mobility, density and charge-carrier in the samples while the resisitivity were measured using a four point probe.

Also during the annealing process an unexpected color change appeared in the crystalline $Mg_{2.4}NiH_4$ samples. This thermochromic effect were investigated with transmission and reflection spectroscopy, which indicates a band gap narrowing. XRD measurements with variable temperature were also performed to investigate if any structural change occurs during heating.

Acknowledgments

First of all I would like to thank the Institute for Energy Technology for this opportunity to work with this interesting subject. Thanks to Trygve, Chang, Zeljka, Erik, Smagul and all other people at IFE for all the help and interesting discussion making these 6 last months very rewarding and successful.

I would also like to thank Dinko Chakarov for all his help and suggestions in writing the thesis and planing my work. My thanks goes also to Maths Karlsson for letting me use the Raman equipment at his department and valuable discussions regarding the results.

Finally I would like to deeply thank my friends and family for all the support and help during all of these years.

Göteborg, Mars 2013

Contents

List of Figures

List of Tables

List of Abbreviations

- TWh - Terawatt hour
- eV - Electron volt
- Mg - Magnesium
- Ni - Nickel
- XRD - X-ray diffraction
- mbar - Millibar
- DC - Direct current
- RF - Radio frequency
- EDS - Energy dispersive x-ray spectroscopy
- GIXRD - Grazing incidence x-ray diffraction
- UV - Ultraviolet
- VIS - Visible
- IR - Infrared
- nm - Nanometer
- TEM - Transmission electron microscopy
- K - Kelvin
- I-V - Current-voltage
- μm - Micrometer
- RBS - Rutherford backscattering spectrometry

1 Introduction

1.1 Background and motivation

Today the ever increasing concern for global climate change and other environmental issues has made new, renewable, energy sources increasingly interesting for research. But a majority of the energy today is still produced using fossil fuels so the renewable energy sources need to increase dramatically to meet the emission goals. One off these renewable sources are photovoltaics,

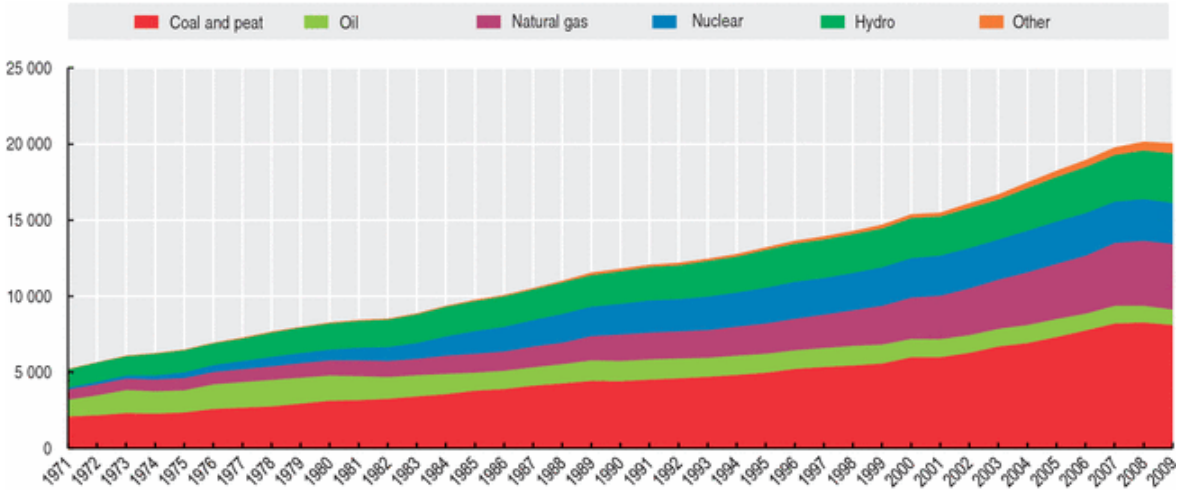

Figure 1.1: The historical contributions of different energy sources to the total energy production in TWh[15]

.

which are semiconductor based devices that convert sunlight to electricity. The first photovoltaic cell based on silicon was constructed in the 1950's with a efficiency of around 6% by Chapin et al at Bell laboratories [2], which was a new world record in 1954 for solar to electric conversion. Since then significant progress has been accomplished and today commercial cells based on silicon have an efficiency around 17-23% which produces electricity at a cost around 2$/watt which is quite an improvement compared to the price of 1500$/watt in 1950. But it is only in the last couple of years that the interest in photovoltaics has done a major breakthrough, the market share has increased from 4 TWh installed in 2005, to 65 TWh 2011. Yet this must be compared to the total energy production in the world which has reached 20000 TWh so the the electricity from photovoltaics is still only a small part of the total energy production, which also is seen in Figure 1.1.

However solar cells have several advantages to other energy sources such as low maintenance and direct conversion from sunlight to electricity, but there are also some disadvantages with

the technique where the biggest obstacle preventing a big expansion in the solar sector today is the production cost. So to make solar cells more attractive the cost must be decreased, this can either be done by making the solar cells more efficiently thus decreasing the area needed. Or to research on cheaper materials and processes to reduce the price per m^2 at the cost of slightly lower efficiency.

An important area of research to both achieve a higher efficiency or cheaper materials this is to find new materials to be used in solar cells. But these new materials also needs to fulfill certain criteria based on the physics behind the solar cells.

1.2 Physical properties of semiconductors and solar cells

To explain how solar cells work a basic understanding of semiconductors is necessary. Semiconductors are a class of materials which exhibit electrical properties in between insulators and conductors; the simplest way to explain these properties is to introduce the concept of band structure. By combining the different discrete energy level for the electrons orbiting the atoms which constitutes the crystal and their positions is it possible to create a structure of allowed and forbidden energies of the electrons in the structure and the relationship between energy and momentum of the electrons.

The forbidden energies constitute a so-called band gap which separate the electrons strongly bound to the core (valence band) and electrons moving around in the lattice (conduction band). To explain the big difference in physical characteristics between metals and insulators/semiconductors the distribution of electrons in the band structure needs to be explained. The distribution of electrons is governed by the so called Fermi-level which says that until this level all allowed states are occupied by electrons according to the Fermi-distribution. For metals the Fermi-level lies inside the conduction band which makes the band half-filled, this enables the electrons to move freely in the conduction band, which is the case for metals where the conductivity is high and the resistance low.

In semiconductors and insulators the Fermi-level lies in the band gap which means that only the valence band is filled and no electrons are in the conduction band at 0K. The difference between semiconductors and isolators lies instead in the magnitude of the band gap; there exists semiconductors which ranges from 0.17eV for InSb up to about 6.2eV for AlN while a typical insulator such as SiO_2 have an even higher band gap of around 8.9eV. The magnitude of the band gap is what gives the semiconductor its specific properties and usages. At 0K a pure semiconductor behaves like an insulator due to that the conduction band is empty, but at higher temperatures the Fermi-distribution of the electrons makes the conduction band partially occupied, in an insulator the band gap is so large that the electrons require large amount of energy to be excited to the conduction band. A schematic overview of the difference is found in Figure 1.2. More background on the theory of semiconductors can be found in the book 'Semiconductor materials:

an introduction to basic principles'[28].

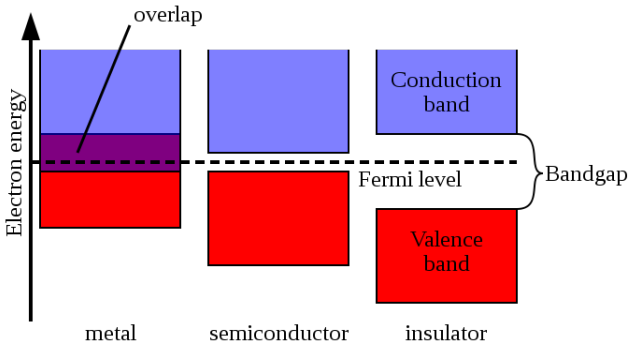

Figure 1.2: Difference in band structure between a metal, semiconductor and insulator.[21]

In a solar cell the band should match the region where most of the photons in the solar spectrum are located, if the band gap is too large the photons will not be able to excite any electrons and if the band gap is too small the excess energy of the photons will convert into heat which reduces the overall efficiency.

When an electron is excited in a semiconductor it leaves behind a hole in the valence band, which will eventually recombine with the electron so that it falls back to the valence band, thus in a solar cell the hole and electron needs to be separated to create a potential which can be used. A term often used in semiconductor physics is 'charge-carrier', which is a particle that carries electrical charge in the semiconductor that can be either a hole or an electron in semiconductors and to determine which carrier type that dominates in a material the term majority charge-carrier is used. The separation of holes and electrons in a 'traditional' solar cell is achieved by changing the concentrations of charge carriers in a material by adding appropriate atoms, creating a so called 'pn-junction' were the electrons and holes are separated through diffusion. With 'appropriate atoms' this means that they should be similar to the semiconductor atom but with one surplus or deficit electron. So the atoms will either donate its extra electron to the conduction band (n-type) or remove one from the valence band (p-type), changing the majority charge carrier. The concentration difference between the two different regions induces an electrical field which drives the charge carriers across the interfaces creating a region which neutralizes the charge difference and makes it possible for the electrons and holes to drift in opposite directions effectively separating the charges, Figure 1.3 illustrates the processes in such a junction.

So which material properties are necessary for a high efficiency photovoltaic cell? First of all the band gap needs to be narrow enough to absorb in the most intensive part of the solar spectrum. The spectra from the sun can be found in Figure 1.4, from this spectra and knowledge of the physical processes in the solar cell Shockley and Quessier calculated the optimal band gap to be 1.4eV [20]. The electrical current is maximized by small band gap but the electrical field is

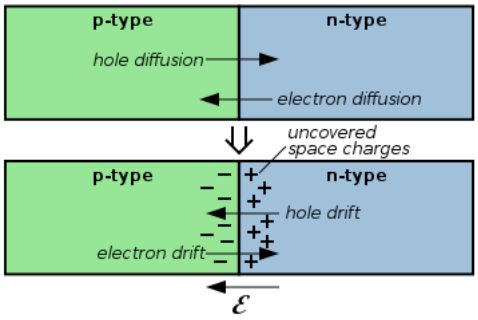

Figure 1.3: The effect of carrier concentration and movement in a pn-junction. P denotes the holes and n denotes the excited electrons.[23]

maximized by a big band gap. Other important optical properties are low reflectivity and low transmission through the material which in other words mean high absorption of photons in the material to reduce the material needed.

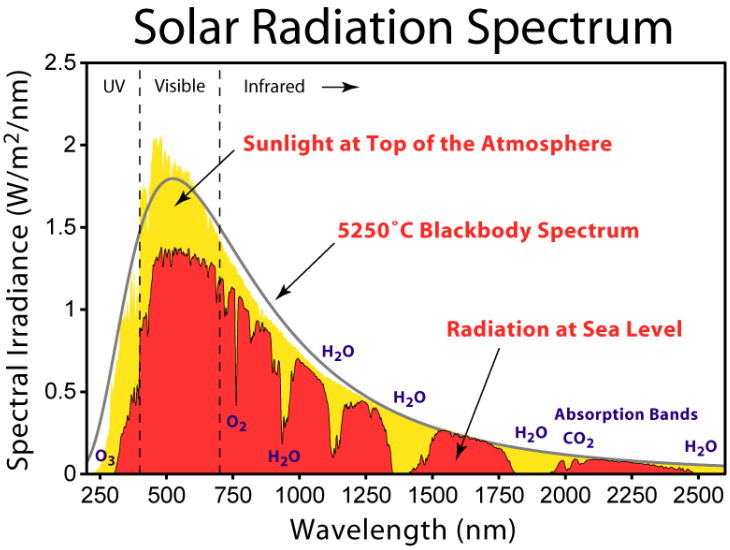

Figure 1.4: The wavelength distribution from the sun at the surface of the earth. [25]

The final material property that needs to mentioned is the transport of charge carriers in the material. As mentioned before the excited electrons have a certain lifetime before they recombines with a hole in the valence band thus loosing a charge carrier which reduces the current. So the conductivity of charge carriers in the material is of outermost importance. To improve the transport of electrons the obstacles for electrons should be few, in other words the resistivity should be low. Physical properties of the material which increases the conductivity are few impurities, grain boundaries and other dislocations. But conductivity is also strongly dependent on the number of charge carriers in the material, more charge carriers gives a better conductivity.

1.3 Goals specifications

The goal of this work is to penetrate the area of the novel semiconductor material Mg_2NiH_4 for photovoltaic applications. First to deposit thin films with uniform composition using reactive sputtering, the structure of these films will be characterized with XRD, Raman spectroscopy and EDS to answer the following questions:

- What is the structure of the deposited films and how does it change upon heating?
- Are there any impurities or defects in the deposited samples?
- How are the hydrogen atoms distributed in the material?

And to investigate whether or not the physical properties, such as band gap and electrical transport properties, makes $Mg_{2.x}NiH_4$ a suitable material in solar cells. The physical properties will be investigated using spectrophotometry, four point probe resistivity measurements and Hall-measurements to investigate the following questions:

- What is the band gap for the different materials, how does it change with composition and annealing?
- What is the resistivity of the samples compared to previous results and how does the resistivity depend on magnesium content and structure of the material?
- What are the physical properties such as mobility and density of the charge-carriers and how does it compared to previous measurements?

Finally the relationship between the structure and the physical properties will be discussed, and also compare these results with previous experiments.

2 Methods & Materials

2.1 Overview

Metal hydrides have in general been of most interest as potential candidates for hydrogen storage but quite lately researchers has started to look into other properties such as electrical properties and optical properties. Mg_2NiH_4 is no exception and it has been extensively investigated for its hydrogen storing properties mostly in the form of nano particles, but the theory of semiconducting metal hydrides were first presented in 1984 by Michèle Gupta [6]. The first experimental work on semiconducting thin films was presented in 2001 by Richardson et al at Lawrence Berkeley National Laboratory.[17] The group were primarily researching if Mg_2Ni could be used as a switchable mirror in the presence of hydrogen and they discovered that the film switched from a shiny metallic state to a transparent semiconducting state in the presence of hydrogen.

The electrical properties of palladium capped Mg_2NiH_4 have investigated by Enache et al in 2004 at the Vrije University [4], but no research of electrical properties has been done on uncapped films.

In 2008 a paper regarding the calculated electronic structure of Mg_2NiH_4 was published by Karazhanov and Ulyashin where they compared theoretical values of Mg_2NiH_4 and silicon which showed promising similarities between Mg_2NiH_4 and silicon. [9] In 2011 Mongstad et al showed that it was possible to synthesize thin films of $Mg_{2.x}NiH_4$ using reactive sputtering for the first time,[13] previously most methods had involved a palladium capping layer. In 2012 the band gap and optical properties were determined experimentally by J.H. Selj et al which confirmed the previous calculations done on $Mg_{2.x}NiH_4$ and concluded that the band gap varies between 1.6eV-2.1eV for different structures of $Mg_{2.x}NiH_4$.[19] Research is still lacking in the areas of semiconducting properties such as carrier types and mobility for uncapped thinfilms.
The structures of Mg_2NiH_4 has been quite extensively researched previously, related to studies of the hydrogen storage properties of the material but not in the form of thin films. The vibrational spectra of Mg_2NiH_4 has also been investigated in the form of nano particles [16], but any research of the thin film Raman spectra is still missing.

2.2 Introduction to the novel semiconductor Mg_2NiH_4

An exciting new material which has the prospect of fulfilling some of the criteria mentioned previously is $Mg_{2.x}NiH_4$, which combines the positive properties of traditional silicon solar cells such as relatively low material cost with the positive properties of thin film solar cells which are high absorption and low material usage. There are also other advantages such as a very appropriate band gap of 1.6eV for certain structural configurations which are quite close to the optimal

band gap of 1.4eV for photovoltaic applications, simpler and cheaper production methods compared to both silicon and thin film solar cells.

As mentioned before Mg_2NiH_4 can obtain three different structures which affects the electrical properties of the material. The first structure is the amorphous as-deposited structure of sputtered thin films. This amorphous structure lacks long ranging periodicity which makes structural characterization difficult but TEM measurements done in previous papers shows that it is actually nano crystalline which means that the materials are consistent of small crystallites with uniform structure but the crystallites are arranged independently to each other which is why there is no long ranging symmetry. The second is the so-called low-temperature (LT) phase it forms when synthesizing Mg_2NiH_4-powders below 510K. This LT phase has a monoclinic structure, where the magnesium atoms are located in the corners and the NiH_4 complex is in the middle. The third structure is the high temperature phase which is achieved when heating up the powder to 510K, it retains the same location of the atoms as in the LT-phase, but changes from a monoclinic to a cubic structure.

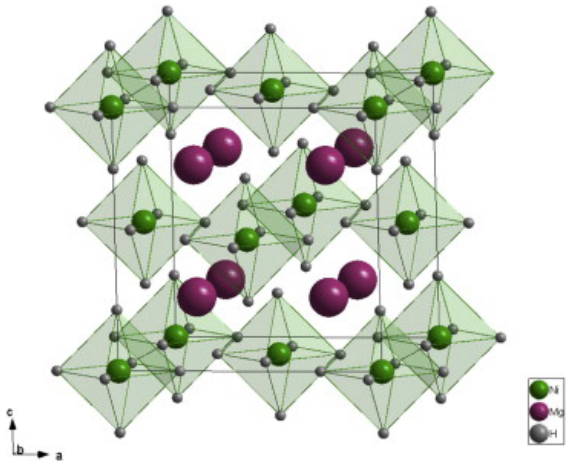

Figure 2.1: The cubic FCC structure of Mg_2NiH_4 [12]. Purple balls represent Mg, green balls represent Ni and gray are the average positions of hydrogen.

The HT phase is found in Figure 2.1, in Figure 2.1 are only the average positions of the hydrogen atoms marked, which have been established by neutron scattering experiments on Mg_2NiD_4 in room temperature [29]. Calculations also show that the hydrogen should form distorted tetrahedral structures around the nickel atoms[5], similar to the structure seen in Figure 2.2.

The difference between the cubic and the monoclinic phase is demonstrated in Figure 2.2, in this figure the hydrogen atoms also assumes more likely positions compared to the structure in Figure 2.1. In thin films the structural behavior is different from nanoparticles, as mentioned before the as-deposited structure is nanocrystalline and when heated up to 590K it undergoes an irreversible change to the cubic HT-phase if there is an excess of magnesium in the samples, the LT-phase has not been detected in thin films yet.

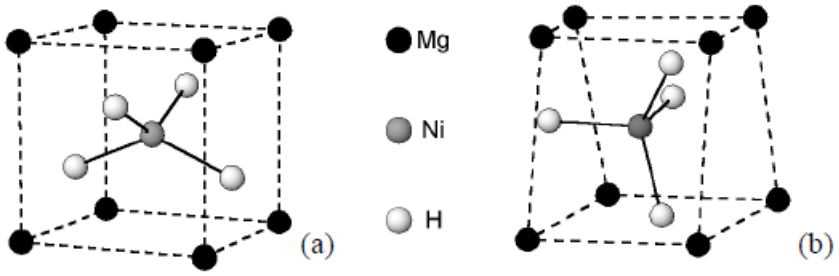

Figure 2.2: Schematic image that demonstrates the difference between cubic (a) and monoclinic (b) structures.

The physical properties that govern the semiconducting properties of Mg_2NiH_4 was first explained by Gupta et al [6], but is also discussed by Garcia et al [5], Karazhanov et al [10] and by Enache et al [4] among others. The general concept of the theoretical work states that the magnesium atoms form Mg-Mg bonds in the material which are thought to form the conducting part in the semiconductor while the NiH_4-complexes will affect the orbitals which opens up the band gap, which means that the material becomes semiconducting. The papers above are focused on the crystalline structures and do not address the amorphous structure.

2.3 Synthesis and sample preparation

2.3.1 Reactive sputtering

The thin films were deposited using a reactive sputtering device by Leybold sputter system A550v7. The sputtering takes place in a vacuum chamber which is filled by a gas mixture of argon and hydrogen up to a pressure of $2{\cdot}10^{-2}$mbar. A strong electrical field is then established between the targets and the substrate which creates a plasma of Ar^+- and H^+ ions, where the positively charged Ar-ions are attracted to the negative surface of the metal targets and hits the surface. The kinetic energy from the Ar-ions are transfered to the target atoms and are kicked out onto the substrate.
For synthesis of the films co-sputtering with two targets activated simultaneously was used to create the desired compositions; a magnesium-target and a Mg_2Ni-target. For co-sputtering in the system used there were two different power sources: A DC-source and a RF-source, so for the depositions in this work the Mg-target was powered by the RF-source and the Mg_2Ni-target was powered by the DC-source. The reason why this setup was chosen was because Ni is magnetic and thus can be effected by the oscillating field, while magnesium is not.

The carrier was set to oscillate in front of the targets with a speed of 0.2 m/s, a schematic of the setup is shown in Figure 2.3. The general process parameters were set according to previous work done with metal hydrides [13] and the power of the magnetrons were adjusted to achieve the different magnesium ratios.

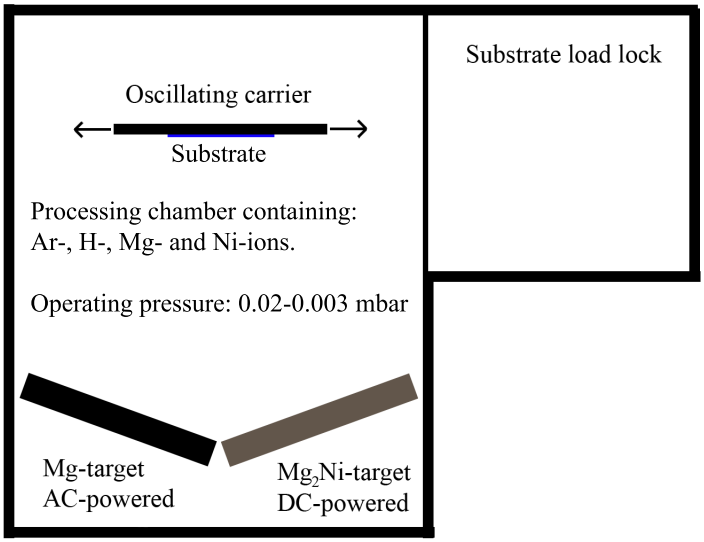

Figure 2.3: A schematic image of the processing chamber.

For EDS, XRD and Raman measurement a layer of $Mg_{2.x}NiH_4$ were deposited on clean glass surfaces and then cut to the appropriate geometry. For the Hall and resistivity measurements

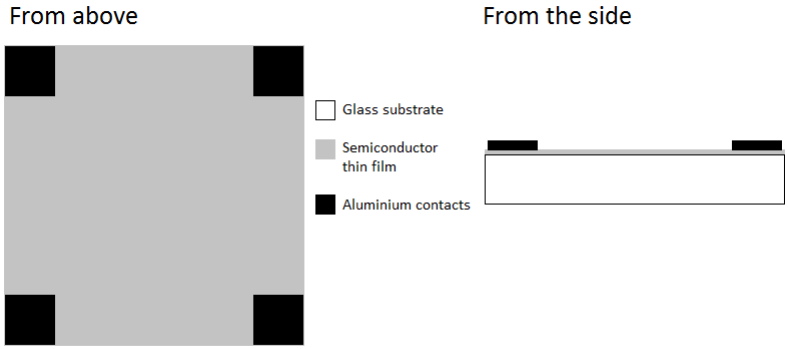

Figure 2.4: Schematic overview of the samples for electrical characterisation.

contacts were also necessary, these were made out of aluminum and the processing parameters for the contacts can also be found in Table 3.1, a schematic of the sample can be found in Figure 2.4. In this case the samples were first cut out, then cleaned before deposition of the

semiconductor film and finally contacts were deposited using a mask made out of single crystal silicon wafers. Two different geomtries were used, the simplest was the van der Pauw-geometry which is seen in Figure 2.4. The second was a so called bridge type geometry which is shown in Figure 2.5. This sample was created using a template made out of an alumina wafer in which the bridge shape was cut with a laser.

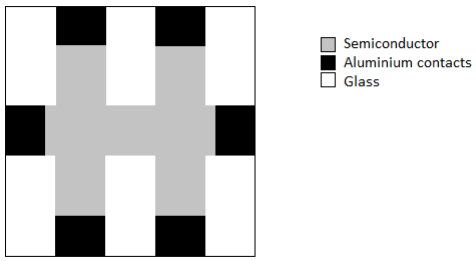

Figure 2.5: Schematic overview of the bridge type-sample used in the PPMS.

2.4 Characterization

2.4.1 Raman spectroscopy

In the case of Mg_2NiH_4 hydrogen plays an important role, so to determine where it is situated in the material is very important. However hydrogen is very difficult to detect with most methods, so Raman spectroscopy was used because it gives the opportunity to detect hydrogen indirectly by the bonds to the other atoms in the material.
Raman spectroscopy is a vibrational method based on the Raman process which is inelastic collisions between photons and molecules or atoms in a material, what happens is that the system absorbs the photon and is excited to a high, 'virtual', energy level. The system then instantly relaxes back to a lower energy level at the same time it emits a photon. When the the system relaxes back two different scenarios can occur:

1. It can relax back to the same energy it had before being excited and emit a photon which has the same energy as the incoming photon. In this case the collision is elastic and the radiation that is released is called Rayleigh scattering.

2. It is also possible that it relaxes back to an energy level with a different energy and emits a photon with changed energy compared to the incoming photon. In this case there are two options: if energy is transfered from the photon to the system the process is called Stoke's scattering while if energy is transfered to the photon it's called anti-Stoke's scattering.

Of the options above it is the second which is interesting in the case of Raman spectroscopy, a graphical representation of the processes can be seen in Figure 2.6. From the energy difference measured in the scattered photons together with the knowledge of the structure, bonds and

atomic species present in the material it is possible to assign the peaks in a Raman spectra to certain motions such as vibrations and translations and determine which atomic species that are involved.

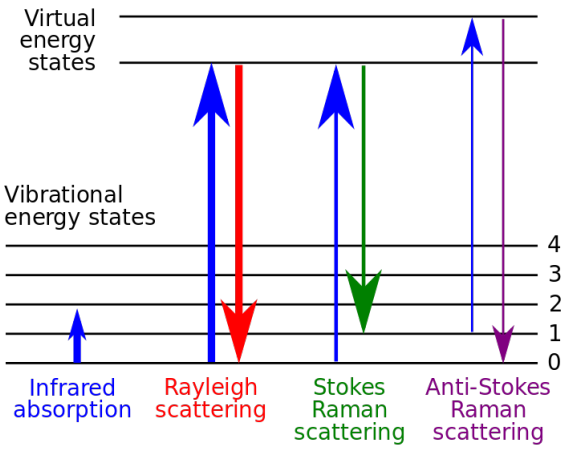

Figure 2.6: The different interband excitation alternatives in atom-photon interactions.[24]

However, not only atomic excitations are possible to occur when light interacts with matter, light can also interacts with the electrons present in the sample. In a semiconductor this interaction between the photons and the electrons is governed by the relationship between the band gap and the laser used in the Raman instrument. If the energy of the laser is higher than the band gap then electrons will be excited to the conduction band, and this could change the appearance of the spectra. The second alternative is if the energy of the laser is smaller than the band gap no electrons will be excited, this is called Raman resonance mode and in this case more modes could be present in the spectra. On a final note, it is also possible to detect other physical properties of the material such as plasmons, crystallite size and in some cases the band gap itself might be visible.

For more information regarding Raman spectroscopy and confocal Raman spectroscopy see the book 'Confocal Raman Microscopy' by Thomas Dieing [3].

2.4.2 Hall-measurements

Hall-measurements is the most commonly used technique to determine physical properties such as mobility, resistivity, charge-carrier density and majority charge carriers in semiconductors. These can all be determined in one single measurement.
As mentioned before in Chapter 1.2 there are two types of charge-carriers in semiconductors and to be able to optimize a photovoltaic cell from a specific semiconductor material the majority charge carrier in that specific material needs to be determined.

The Hall-effect was discovered in 1879 by Edwin Herbert Hall, and is in short the effect a magnetic field has on the current flowing in a conductor or semiconductor. In a conductor without any influence of a magnetic field the electrons flow in a straight line from one end to the other. While if a strong magnetic field is introduced perpendicular to the current, the electrons will be influenced by the so called Lorentz force which will effectively alter the movement. This change can be described as if the electron trajectories are slightly bent, which is illustrated in Figure 2.7. This change also lead to an accumulation of charge carriers on one side of the material thus inducing an electrical field perpendicular to the applied current and the magnetic field, which is called the Hall-voltage. A schematic view of a Hall-setup can be found in Figure 2.7. If the

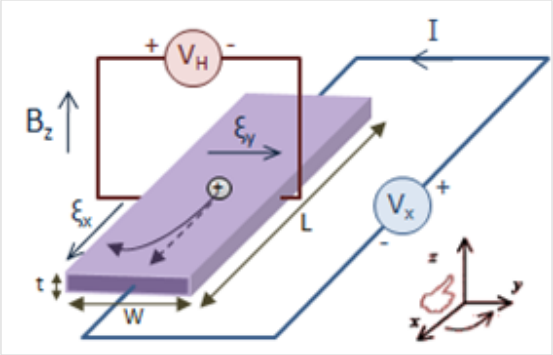

Figure 2.7: Illustration of the general setup for Hall-measurements, I = The current sent through the sample, V_X=Voltage applied through the sample, B_Z = Magnetic field perpendicular to the current, V_H = The measured Hall-voltage, t = thickness of sample. [26]

Hall-voltage is measured it is possible to calculate the so called Hall-coefficient which is defined as

$$R_H = \frac{E_y}{j_x B_Z} \tag{2.1}$$

In which all of the variables are known: E_y is the measured Hall-voltage, j_x is the current and B_Z is the applied magnetic field. But to evaluate what this coefficient says about the material, the applied current is defined as $j_x = ne^2\tau E_x/m$ where n is the number of charge carriers, e is the elemental charge, τ is the collision frequency between the electrons and m is the electron mass. If this expression is inserted into 2.1 the following result is obtained:

$$R_H = -\frac{1}{ne} \tag{2.2}$$

Where n is the density of charge-carriers and finally Equation 2.2 shows that the Hall-coefficient will shift sign depending on the sign of the charge-carrier. For electrons the charge, e, is positive by definition and for holes the charge becomes negative.
So by knowing the current fed to the sample and the magnetic field while measuring the transverse electrical field, E_y, is it possible to determine the type of carriers in the material by looking

at the sign of the Hall-coefficient and the concentration of charge carriers depending on the magnitude of the coefficient. [11]

Some samples though can be problematic, if the carrier concentration is high the coefficient is very small and combined with a small current j_x can effectively lower the Hall-coefficient below the sensitivity range of the device.

For more background and theory regarding Hall-effect and charge carriers can be found in the book 'Semiconductor materials: an introduction to basic principles' [28].

Two different setups were used to try and determine the Hall-effect and properties.
The first and most frequently used was a device from MMR with a H-50 electrical controller and the K-20 temperature controller, the device uses a magnetic field of 14 Tesla and DC to power the magnets and measurements. In this device the sample was required to use the so called van der Pauw gemotry, which can be seen in Figure 2.4. In the MMR device the probes were not soldered directly unto the contacts which simplified operations but decreased the quality of the connection. The second device that was tried was from PPMS which supports an alternating magnetic field and AC-power use in the measurements. In this device the probes was soldered onto the contacts for better connection and a bridge type geometry was used to increase the sensitivity, which can be seen in Figure 2.5.

2.4.3 X-ray diffraction

X-ray diffraction (XRD) was used to determine the crystal structure of the thin films. It is a fairly quick technique which can be used to determine which structure is present but also physical information such as distance between different atomic layers which also gives information about the dimensions of the unit cell.
XRD is a common technique to identify the structure of crystalline materials, using the theory of atom - x-ray and x-ray - x-ray interaction. When a material is illuminated by an x-ray source the energy intensive x-ray photons are reflected by crystal planes in the material. The photons then, depending on the structure of the material, interact with each other. The simplest way of describing this is by using Bragg's Law which gives the diffraction conditions,

$$2d_{\text{hkl}}sin(\theta) = n\lambda \tag{2.3}$$

Where d_{hkl} is the distance between the atomic planes in the material, θ is the angle between the sample and the intensity peak, n is an integer and finally λ is the wavelength of the radiation used in the measurement. However, for a fuller understanding and predictions of intensities advanced Fourier analysis is required.

There are several different setups for XRD-analysis and in this report two slightly different setups were used: Grazing Incidence XRD and XRD. The difference in the setups is the angle of incidence for the x-ray beam, for the ordinary XRD the incidence angle was 5 degrees while in

the GIXRD setup it was 0.5 degrees. The GIXRD setup is more appropriate for thin-films while XRD is more suitable for bulk materials, however for the setup with controllable temperature only the XRD setup was available. In this setup there was a sample holder made out of a Pt-Ru alloy, this sample holder was also crystalline so in these experiments several background peaks can be observed.

2.4.4 Energy dispersive x-ray spectroscopy

To confirm the compositions of the films, Energy Dispersive X-ray Spectroscopy or simply EDS, was used because it is a fairly easy and well known method. The accuracy of EDS has been compared RBS measurements on Mg_2NiH_4-thin films and it has proven to give the same results [18]. The electron microscope used in this paper was a Hitachi S-4800 equipped with a Noran System SIX detector for EDS measurements.
In EDS high energy electrons are sent towards the atoms and kicks out electrons orbiting the cores in the inner shells, an electron in an outer shell then subsequently falls in to take its place. In this process the electron looses potential energy which is emitted as x-ray radiation. The energy of the emitted photons depend on which atomic specie, from which shell it falls from and also to which shell. A schematic overview of the process can be found in Figure 2.8

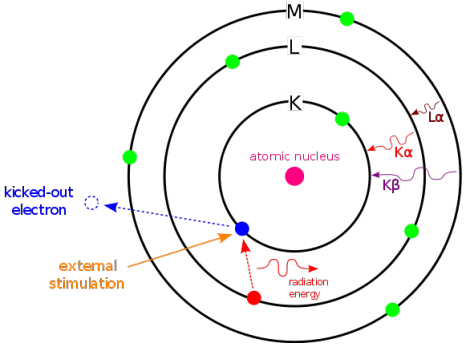

Figure 2.8: Schematic overview of the processes involved in EDX.[22]

The perhaps biggest drawback of EDS is that the electronic configurations of many elements are quite similar, this leads to that the energy of the emitted X-rays are in some cases also quite similar. This means that if certain elements are present in a sample it's impossible to quantify the amounts of these elements. The second major drawback is that lighter materials such as hydrogen are invisible in the EDS-spectra. However magnesium and nickel are fairly heavy and does not overlap significantly with other atoms which makes it possible to detect and quantify them.

2.4.5 Band gap calculations

To calculate the band gap in the material, a method developed by E. Centurioni was used. It uses the transmission and reflection spectra with the refractive index of the material to calculate

the actual absorption and band gap. To get the refractive index a technique called ellipsometry is used, however no such measurements were conducted in this work so previous ellipsometry measurements were used. Unfortunately, refractive index data have only been measured for certain magnesium contents and structures such as: a-$Mg_{1.9}NiH_4$, a-$Mg_{2.1}NiH_4$, c-$Mg_{2.2}NiH_4$, a-$Mg_{2.3}NiH_4$ and c-$Mg_{2.4}NiH_4$. So to calculate the band gap for the compositions where no refractive index data were available the closest composition was chosen.

The algorithm in the program is based on the internal light flux in multilayered materials, instead of the light intensity which is used in other techniques. However in this work the program was used to calculate the band gap, to calculate the optical band gap the reflectance, absorption and refractive index data was used to calculate the so called Tauc plot. In the Tauc plot the linear section is identified and the optical band gap is calculated by letting the tangent of the linear intersect the x-axis.

More information about the method can be found in the paper 'Generalized matrix method for calculation of internal light energy flux in mixed coherent and incoherent multilayers' by E. Centurioni. [1]

2.4.6 Spectrophotometry

Spectrophotometry was the technique used to obtain the absorption and reflection spectra of the deposited samples. This technique was used because it's essentially the only way to obtain these spectra. It is also a very common technique in almost all research areas were optical properties are interesting. The technique is straight forward and simple: first two optical cords are mounted on the sample holder one connected to the light source and the other connected to the light detector. The next step is to create a reference, both without the light source and then a reference of the light source itself, now the sample is put in place and the transmission and reflection spectra is acquired simply by changing the location of the light source.

To treat the data the program 'Spectrasuite' was used with an acquisition time of 0.3 s, and three averaged acquisitions for each result. The light sources used were a UV-VIS source and a infrared source the UV-VIS operated in the region 198-998 nm and the infrared 899-1719 nm.

3 Results

3.1 Synthesis of $Mg_{2.x}NiH_4$

Thin-films with three different magnesium contents were synthesized using reactive co-sputtering described in Chapter 2.3 with a Leybold sputter system A550v7. The different compositions were $Mg_{2.0}NiH_4$, $Mg_{2.2}NiH_4$ and $Mg_{2.4}NiH_4$, the settings used to achieve the different compositions can be found in Table 3.1.
The hydrogen content was not experimentally determined in this thesis, but the nickel:hydrogen

Table 3.1: General processing parameters for deposition of the different samples.

Desired Material	$Mg_{2.0}NiH_4$	$Mg_{2.2}NiH_4$	$Mg_{2.4}NiH_4$	Aluminium
Effect of Mg-target (W)	750	875	900	N/A
Effect of $NiMg_2$-target (W)	800	700	600	N/A
Effect of aluminium target (W)	N/A	N/A	N/A	3000
Hydrogen flow (sccm)	60	60	60	0
Argon flow (sccm)	140	140	140	200
Processing pressure (mbar)	$2{\cdot}10^{-2}$	$2{\cdot}10^{-2}$	$2{\cdot}10^{-2}$	$3{\cdot}10^{-3}$
Deposition time (minutes)	100	105	90	30

ratio is assumed to be close to 1:4. This assumption is based on the fact that the obtained XRD patterns is consistent with Mg_2NiH_4 and also due to the fact that computational studies shows that Mg_2NiH_4 is the only stable configuration and if there is a lack of hydrogen atoms then there will be regions of Mg_2NiH_4 and regions of metallic Mg_2Ni [5]. However it is possible that there could be small variations in the hydrogen concentration, but this and the possibility of metallic Mg_2Ni-regions will be discussed later. The thickness of the films were measured using a profilometer, KLA-Tencor alpha-step 200, to 400 nm for $Mg_{2.0}NiH_4$, 400 nm $Mg_{2.2}NiH_4$ and 410 nm for the $Mg_{2.0}NiH_4$ sample.

Samples for electrical characterisation were made by the $Mg_{2.0}NiH_4$ and $Mg_{2.4}NiH_4$ samples, the aluminum contacts deposited was determined to have a thickness of 1 micrometer.
To confirm the compositions EDS was used. The results are presented in Table 3.2 as mean values of three measurements over different areas on the samples.

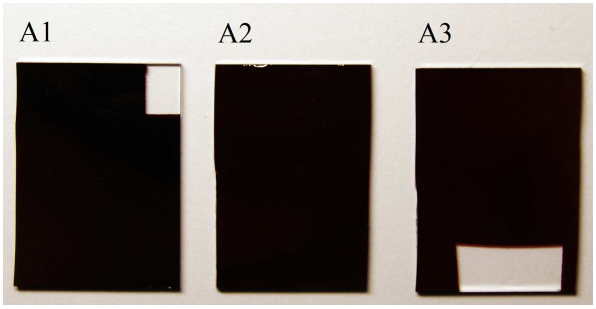

Figure 3.1: Image of the deposited $Mg_{2.0}NiH_4$-thin films; A1 - As-deposited, A2 - Annealed at 220C and A3 - Annealed at 290C.

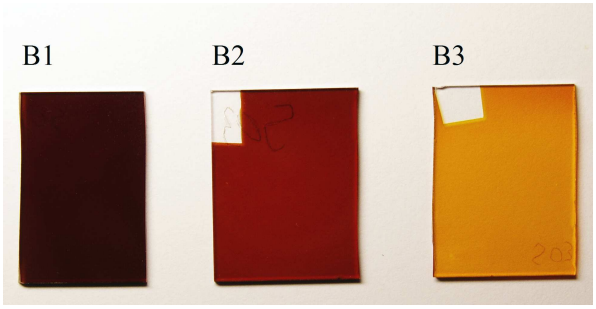

Figure 3.2: Image of the deposited $Mg_{2.2}NiH_4$-thin films; B1 - As-deposited, B2 - Annealed at 220C and B3 - Annealed at 290C.

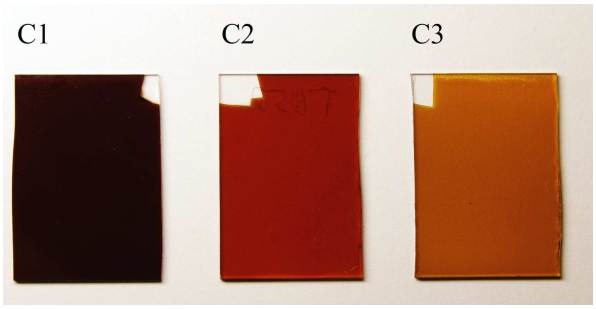

Figure 3.3: Image of the deposited $Mg_{2.4}NiH_4$-thin films; C1 - As-deposited, C2 - Annealed at 220C and C3 - Annealed at 290C.

Table 3.2: EDS results for the Mg and Ni composition of the synthesized films.

Element (atomic-%)	$Mg_{2.0}NiH_4$	$Mg_{2.2}NiH_4$	$Mg_{2.4}NiH_4$
Mg	9.73	23.76	8.72
Ni	4.96	10.87	21.09
Mg/Ni ratio	1.96	2.18	2.42

3.2 Structural determination

3.2.1 X-ray diffraction

The settings used for the XRD and GIXRD measurements conducted can be found in Table 3.3.

Table 3.3: Settings for the XRD & GIXRD setups

Setup	Incident angle	Scan speed [seconds/step]	Increment [degrees/step]
GIXRD	0.5	1.5	0.01
XRD	5	0.4	0.02

GIXRD results were obtained for all compositions, samples A1 - A3, B1, B2, C1 and C2 didn't give any diffraction pattern, which is expected from previous research. These samples will be described to be amorphous, however measurements with TEM shows that the as deposited state is actually consistent of nanocrystals of the monoclinic structure [13]. The two diffraction patterns that were obtained from sample B3 and C3 are presented in Figure 3.4 and compared with litterature data in Table 3.4. Where 2theta simply is the diffraction angle multiplied by two.

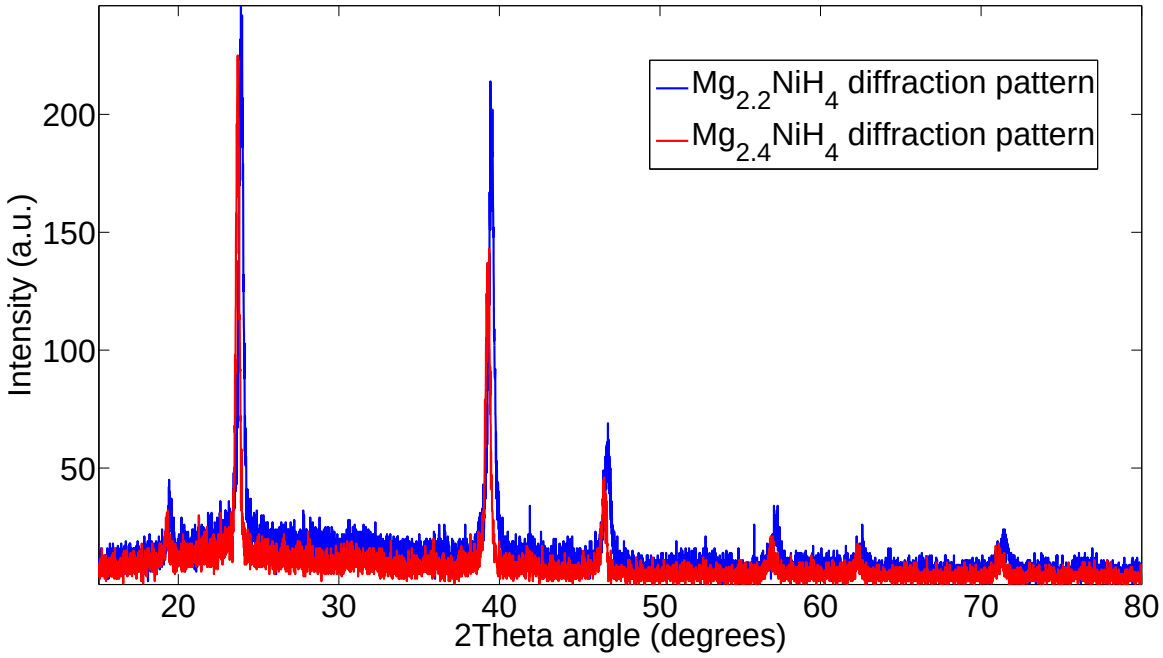

Figure 3.4: The XRD-patterns of the crystalline $Mg_{2.4}NiH_4$ and $Mg_{2.2}NiH_4$ thin films

Table 3.4: Comparison of obtained peaks of the $Mg_{2.4}NiH_4$ and $Mg_{2.2}NiH_4$ sample with literature data for cubic Mg_2NiH_4 [29].

Obtained GIXRD diffraction peaks (2theta)			
$Mg_{2.4}NiH_4$	$Mg_{2.2}NiH_4$	Reference data (2theta)	Plane assignment
19.43	19.53	-	-
23.70	23.90	23.68	111
39.26	39.44	39.14	220
46.52	46.67	46.28	311
57.04	57.1	56.58	400
62.32	62.67	62.2	331
71.3	71.47	70.96	442

To investigate if any structure change occurs at higher temperatures XRD measurements of $Mg_{2.4}NiH_4$ were conducted at 300C. One should note that in the XRD measurement a higher angle of incidence is used compared to GIXRD, which leads to that the peaks with higher indices should not be visible in the spectra. There is also a slight difference in the alignment so the XRD results at room temperature differ slightly from the GIXRD results at room temperature. The sample holder leaves a significant background signal which is marked in the spectras.

Table 3.5: Comparison of obtained peaks at 300C and room temperature for $Mg_{2.4}NiH_4$ with reference data [29].

Obtained diffraction peaks (2theta)			
Room temperature	300C	Reference data (2theta)	Plane assignment
-	17.18	-	-
23.82	23.34	23.68	111
39.47	38.8	39.14	200, background
46.77	45.83	46.28	311, background
-	67.37	62.2	background
-	81.36	-	background

No major shifts can be seen at 300C, however two big differences can be seen:First is the broad peak that appears at 17 degrees in the XRD spectra at 300C. The second major difference is otherwise that the unidentified peak at 19 degrees in the GIXRD spectra is missing in the XRD spectra both at room temperature and at 300C. Also worth noting is that signal from the sample

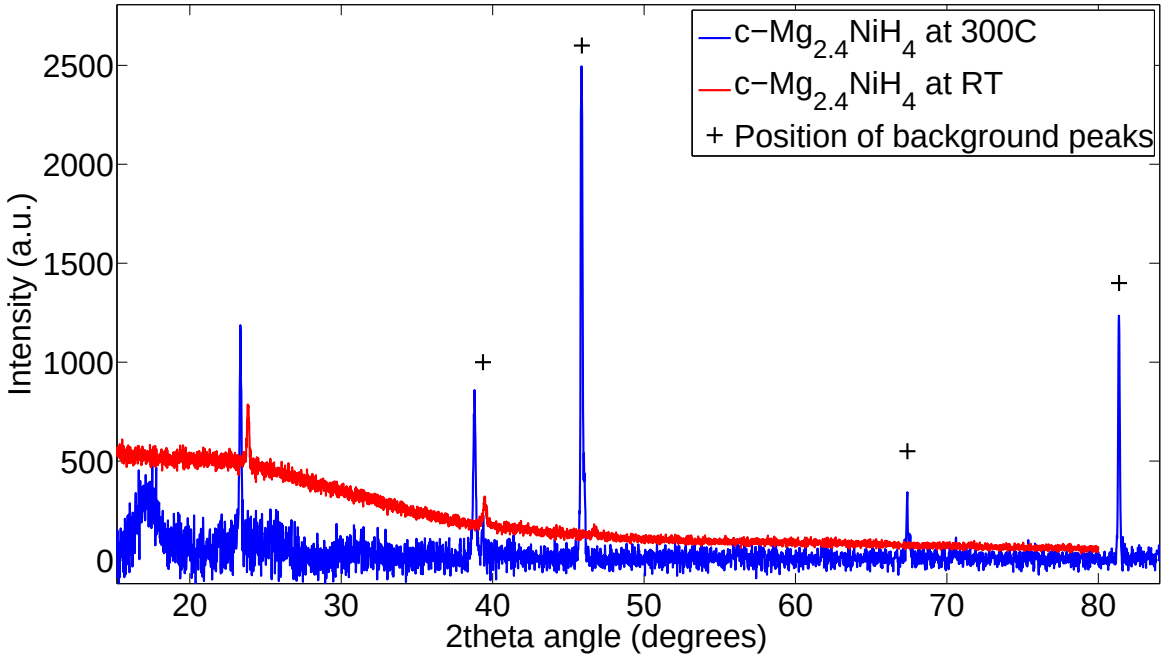

Figure 3.5: Comparison of the XRD-patterns for $Mg_{2.4}NiH_4$ at 300C and at room temperature with the background from the sample holder marked.

holder unfortunately almost coincides with the peaks from the sample which makes it hard to evaluate the intensity of the signal from the sample.

3.3 Electrical properties of $Mg_{2.0}NiH_4$ and $Mg_{2.4}NiH_4$

It proved very difficult to get any Hall-results for the samples, attempts were made att two different setups but neither the MMS or the PPMS could give any clear results with regard to charge carrier and mobility. Attempts were also made on the bridge type geometry but the same problem appeared.

Table 3.6: Result of Hall-measurements performed on a crystalline $Mg_{2.4}NiH_4$ sample at 325K.

Mobility (cm^2/Vs)	Density (cm^{-3})	Hall-coefficient (cm^3/Coulomb)	Charge-carrier
0.2152787	$7.82 \cdot 10^{15}$	798.5893	holes
-0.6389735	$-2.62 \cdot 10^{15}$	-2382.292	electrons
1.472012	$1.14 \cdot 10^{15}$	5484.745	holes
1.053373	$1.59 \cdot 10^{15}$	3930.077	holes
0.2598856	$6.43 \cdot 10^{15}$	971.0396	holes
-1.656226	$-1.01 \cdot 10^{15}$	-6182.084	electrons
-2.006044	$-8.36 \cdot 10^{14}$	-7465.271	electrons
-0.906009	$-1.85 \cdot 10^{15}$	-3370.273	electrons
-2.304747	$-7.29 \cdot 10^{14}$	-8566.501	electrons
0.3849843	$4.35 \cdot 10^{15}$	1434.723	holes
0.717042	$2.33 \cdot 10^{15}$	2675.491	holes
-1.986795	$-8.43 \cdot 10^{14}$	-7405.526	electrons
1.30E-02	$1.29 \cdot 10^{17}$	48.3511	holes
0.9692526	$1.73 \cdot 10^{15}$	3610.303	holes
1.588597	$1.05 \cdot 10^{15}$	5921.307	holes

A typical result is presented in Table 3.6 to demonstrate the problem that occurred in the process: Half of the measurements indicate holes as charge carriers while the other halv indicates electrons. This measurement was done at 325K for a quadratic van der Pauw sample of crystalline $Mg_{2.4}NiH_4$. To get the resistivity a I-V curve was obtained with a four point probe described in Chapter 2.4.2. The measurements were done on van der Pauw-samples and the result is the average of 4 measurements between the different contacts. To get the resistivity the slope of the I-V curved that was obtained was multiplied according to the following formula:

$$\rho = \frac{\pi d}{ln2} R_{\text{measured}} \tag{3.1}$$

Where d is the thickness of the sample and $R_{measured}$ is the measured resistance.

Table 3.7: Measured resistivities of the deposited films in ohm*cm.

	$Mg_{2.4}NiH_4$	$Mg_{2.0}NiH_4$
As-deposited	$1.1 \cdot 10^4$	337
Annealed at 220C	$5 \cdot 10^5$	10^6
Annealed at 290C	$1.1 \cdot 10^4$	$1.1 * 10^7$

The result in Table 3.7 shows that the resistance is strongly dependent on annealing temperature where the $Mg_{2.0}NiH_4$ shows the most drastic increase upon heating going from the lowest to the highest resistivity. It seems also as if deviations from $Mg_{2.0}$ results in increased resistivity. To get a feeling if these resistivities should be considered high or low among semiconductors one can compare them with the resistivities of silicon. Intrinsic, or pure, silicon have a resistivity of about 10^5 ohm*cm which decreases to 10^{-3} for heavily doped silicon. So the measured resistivities lies in that region except for the annealed $Mg_{2.0}NiH_4$ samples.

3.4 Calculated bandgaps of the deposited thin films

The band gaps were calculated for all compositions and also for the heated state.

Table 3.8: Calculated band gaps of the deposited films in electron volt.

	$Mg_{2.4}NiH_4$	$Mg_{2.2}NiH_4$	$Mg_{2.0}NiH_4$
As-deposited	1.6	1.73	1.53
Annealed at 220C	1.85	1.83	1.69
Annealed at 290C	2.04	2.15	1.74
Heated crystalline sample	1.8	-	-

The band gap of the as-deposited states are roughly the same independent of magnesium content, and the general trend is that the band gap increases with annealing. Which is most strongly seen where there is a structure change from amorphous to crystalline. Upon heating the band gap seems to shrink compared to the state at room temperature.

3.5 The thermochromic effect in $Mg_{2.4}NiH_4$

When the $Mg_{2.4}NiH_4$ samples with crystalline structure were heated up to around 200C a reversible change in color were observed, which can be seen in Figure 3.6. The change in transmission and reflection were also recorded, which is demonstrated in Figure 3.7 and 3.8.

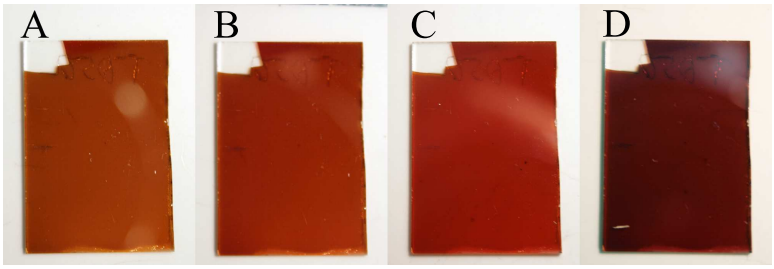

Figure 3.6: Image of the $Mg_{2.4}NiH_4$ sample at different temperatures; A: Room temperature, B: 100C, C: 200C, D:300C

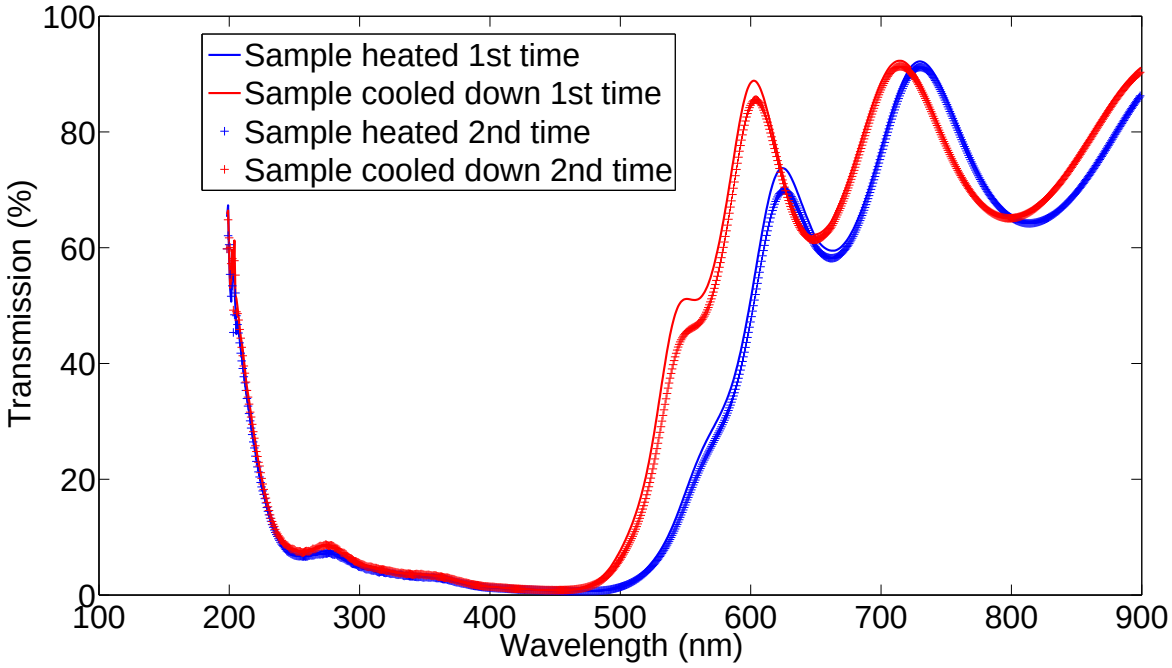

Figure 3.7: Transmission spectra of $Mg_{2.4}NiH_4$ sample heated to 300C and at room temperature.

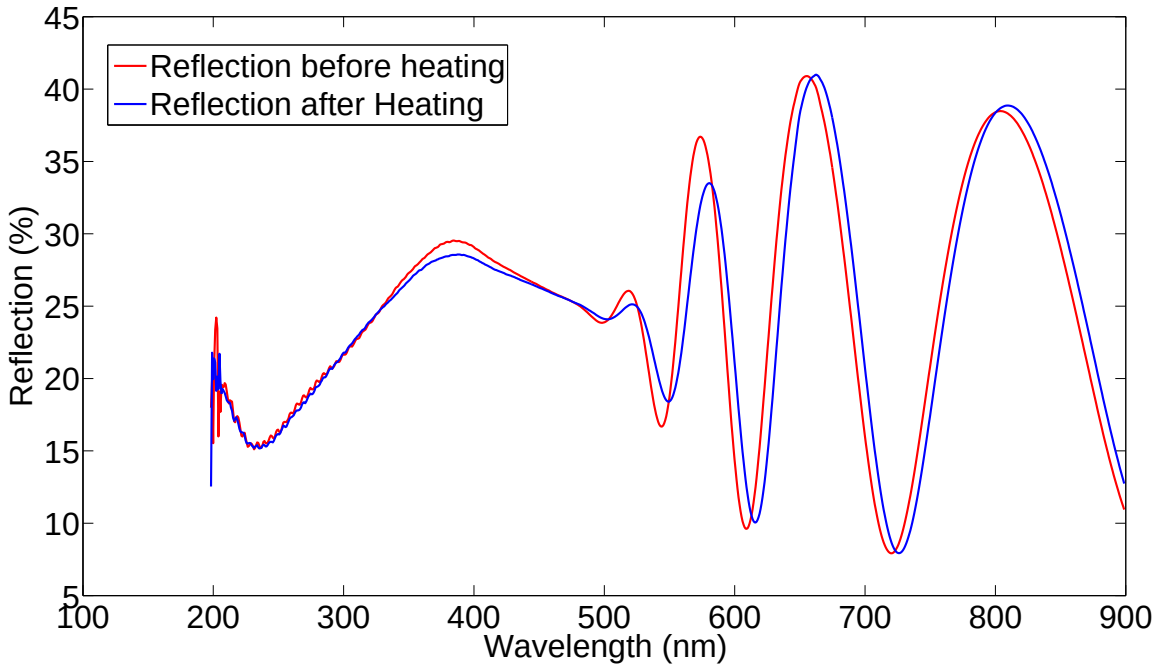

Figure 3.8: Reflection spectra of $Mg_{2.4}NiH_4$ sample heated to 300C and at room temperature.

As seen the reflection spectra hardly changes upon heating, however the transmission spectra changes drastically upon heating which is seen as a color change in the samples and a narrower band gap in the band gap calculations.

3.6 Raman spectra results

For the following Raman measurements the settings used can be found in Table 3.9.

Table 3.9: Settings used for Raman measurements

Wavelength	Accumulation	Time	Objective	Hole	Slit	Grating (lines/mm)
632.8 nm	8	600	100x	200 μm	200 μm	1800

Below are spectra from two different regions of interest, first is the low energy region and the region were the translation modes, phonons and acoustic modes are found. To identify the peaks an article by Parker et al is referred to, one should however keep in mind that the reference peaks are from nanoparticles.

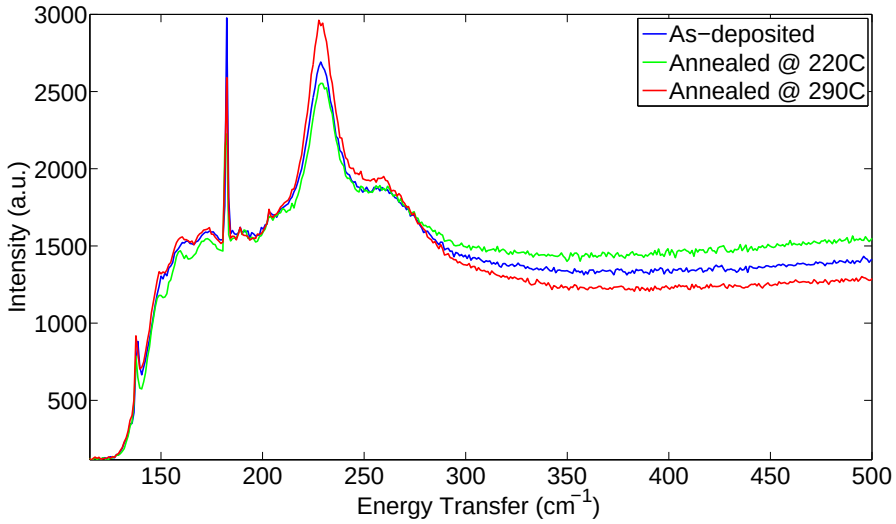

Figure 3.9: Low energy region of the Raman spectra $Mg_{2.0}NiH_4$-thin film.

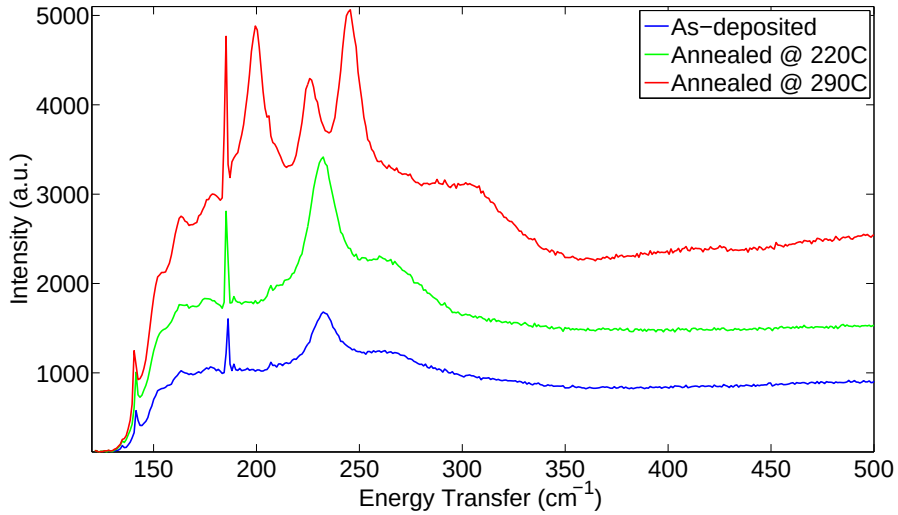

Figure 3.10: Low energy region of the Raman spectra $Mg_{2.2}NiH_4$-thin film.

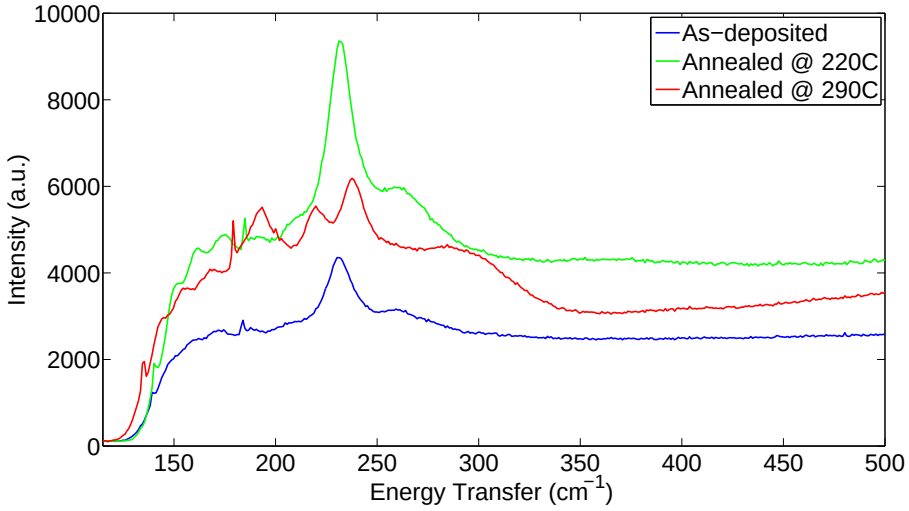

Figure 3.11: Low energy region of the Raman spectra $Mg_{2.4}NiH_4$-thin film.

From Figure 3.9, 3.10 and 3.11 one can see that the spectra from the as-deposited samples look very similar but is quite different from the reference spectra. No change is seen in the $Mg_{2.0}NiH_4$ upon heating, however the $Mg_{2.2}NiH_4$ and $Mg_{2.4}NiH_4$ samples annealed at 290C is quite different and are more similar to the reference spectra while the same samples only annealed at 220C almost retains the spectra of the as deposited samples.

However the Ni-H bonds that were of particular interest have a higher excitation energy, the result from the measurements in the energy region were these peaks should appear is found in Figures 3.12 and 3.13. No peaks were found in this interval for the $Mg_{2.0}NiH_4$ samples, therefor only the results from the $Mg_{2.2}NiH_4$ and $Mg_{2.4}NiH_4$ samples are included.

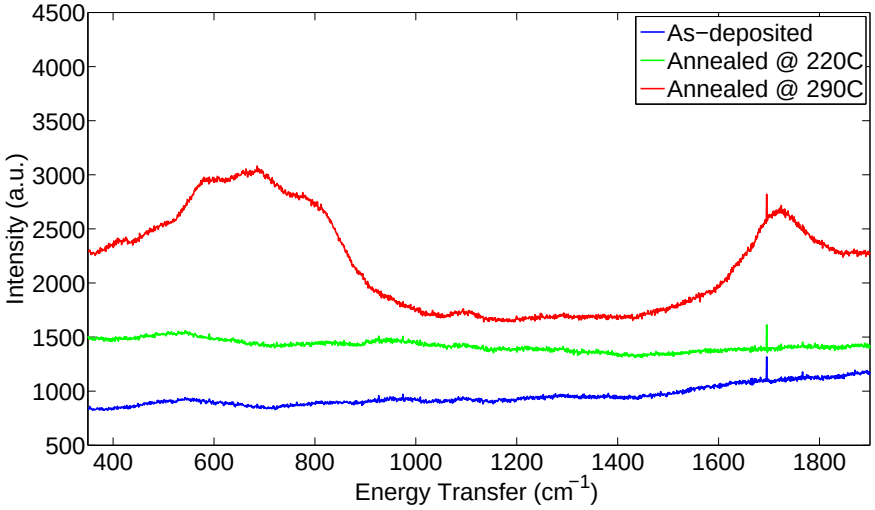

Figure 3.12: The Ni-H region of the Raman spectra $Mg_{2.0}NiH_4$-thin film.

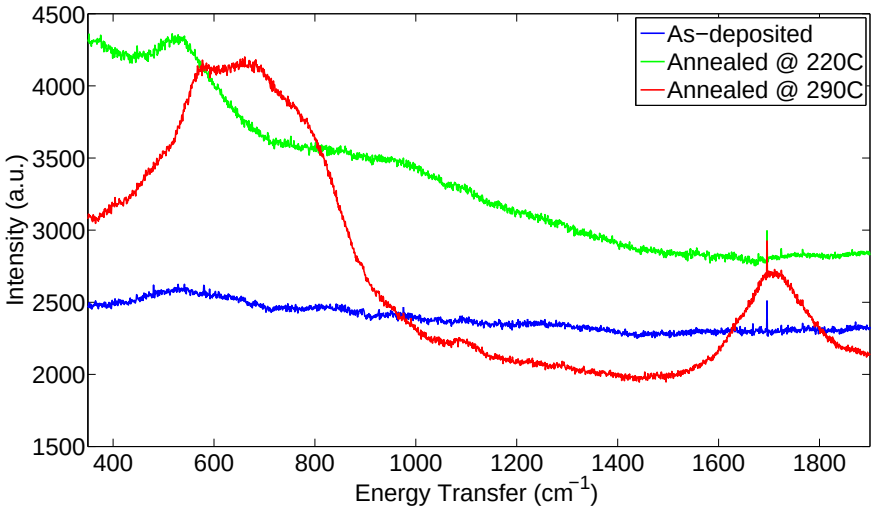

Figure 3.13: The Ni-H region of the Raman spectra $Mg_{2.4}NiH_4$-thin film.

The plots in Figures 3.12 and 3.13 show no signs of Ni-H bonds in the amorphous samples, it is first in the crystalline samples that the Ni-H bonds appear. No peaks from OH-bonds or other impurities are not present in any of the samples.

In Tables 3.10, 3.11 and 3.12 summaries of the obtained peaks compared to the literature data is listed for each composition

Table 3.10: Comparison of obtained Raman-spectras for $Mg_{2.0}NiH_4$ with reference [16].

Reference peak and assignments	Obtained peaks for the different structures
1691 strong, vNi-H	-
791 medium, dNi-H	-
654 medium, dNi-H	-
474 weak, Libration	-
396 weak, Libration	-
299 weak, Translation	-
274 weak, Translation	258 shoulder (all samples)(?)
241 strong, Mg translation	-
224 weak, Translation	228 very strong (all samples)
197 very strong, Mg translation	-
-	182 very strong
179 weak, Translation	172 weak (all samples)
-	158 weak (Annealed samples)
154 weak, Acoustic	150 weak (Annealed samples)
-	140 weak (all samples)

Table 3.11: Comparison of obtained Raman-spectras for $Mg_{2.2}NiH_4$ with reference [16].

Reference peak & assignment	Obtained peaks for the different structures
1691 strong, vNi-H	1723 medium (290C)
791 medium, dNi-H	776 shoulder (290C)
654 medium, dNi-H	684 medium (290C)
-	594 medium (290C)
-	513 shoulder (290C)
-	416 weak (290C)
474 weak, Libration	-
396 weak, Libration	-
299 weak, Translation	287 (290C), 260 (220C, as-deposited) shoulder
274 weak, Translation	-
241 strong, Mg translation	244(290C), 232 (220C, as-deposited) very strong
224 w, Translation	227 (290C) strong
-	207 (all samples) shoulder
197 very strong, Mg translation	199 (290C) strong
-	185 strong (all samples)
179 weak, Translation	179 (290C), 175 (220C, as-deposited) weak
-	162 (290C), 163 (220C, as-deposited) weak
154 weak, Acoustic	154 (all samples) shoulder
-	140 (all samples) weak

Table 3.12: Comparison of obtained Raman-spectras for $Mg_{2.4}NiH_4$ with reference [16].

Reference peak & assignment	Obtained peaks for the different structures
1691 strong, vNi-H	1707 medium (290C)
791 medium, dNi-H	750 shoulder (290C)
654 medium, dNi-H	661 strong (290C)
-	567 medium (290C)
474 weak, Libration	-
396 weak, Libration	-
299 weak, Translation	284 (290C), 260 (220C, as-deposited) shoulder
274 weak, Translation	-
241 strong, Mg translation	238 (290C) very strong
224 w, Translation	219 (290C) strong
-	200 (290C) weak
193 very strong, Mg translation	193 (290C) strong
-	179 strong (*)
179 weak, Translation	-
-	170 weak
154 weak, Acoustic	155, weak (290C)
-	147 shoulder

One of the questions asked was if there is any oxides present in the thin films, since no oxides were found in the other samples measures were taken to try and increase the oxide content. To achieve this two $Mg_{2.4}NiH_4$-samples, one annealed at 290C and one as-deposited, were oxidized in distilled water for 3 hours before Raman spectras were acquired and compared to the unoxidized films, which can be seen in Figure 3.15 and 3.14.

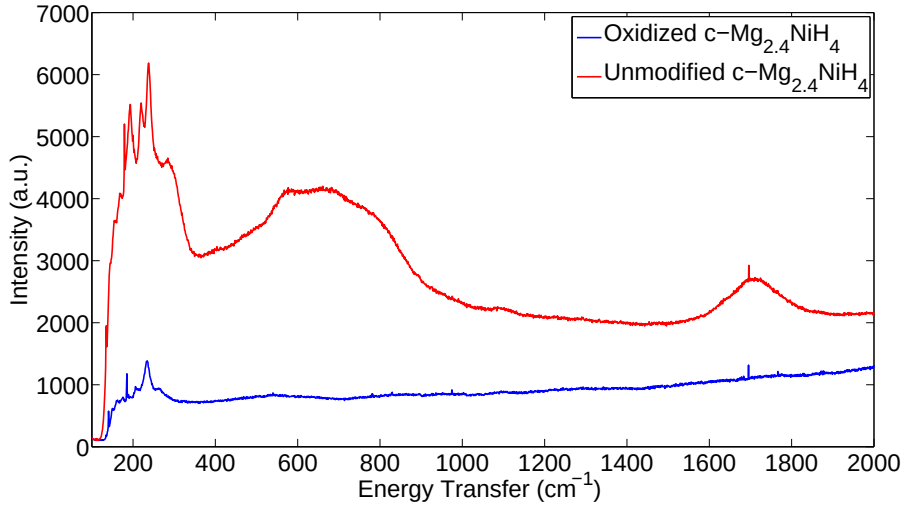

Figure 3.14: The Raman spectra of oxidized crystalline $Mg_{2.4}NiH_4$ compared to the unmodified sample.

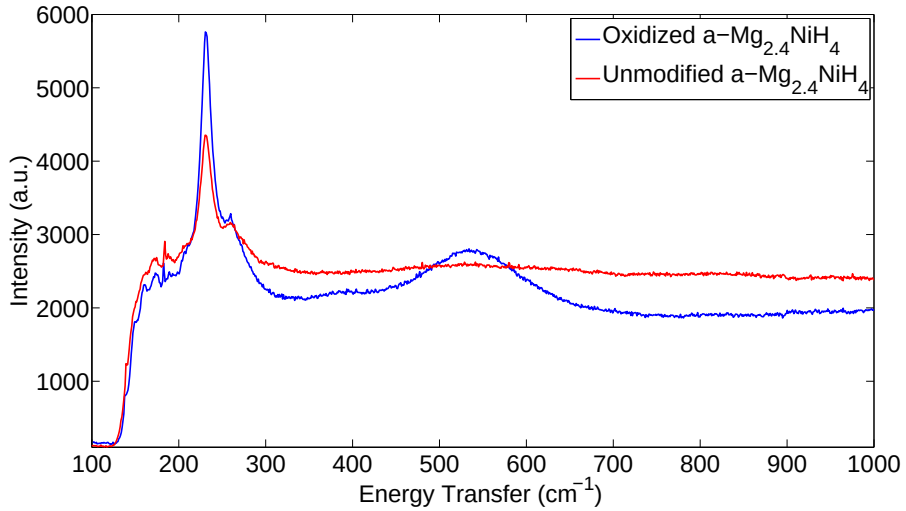

Figure 3.15: The Raman spectra of oxidized amorphous $Mg_{2.4}NiH_4$ compared to the unmodified sample.

In Figure 3.14 the Ni-H bonds disappear in the oxidized samples, the spectra also looks more like the amorphous samples in the low energy region. But no OH-groups or other oxides are visible in the spectra. However in Figure 3.15 a new peak appears in the spectra from the oxidized sample, which seems to represent bonds not seen in any of the previous samples.

Finally one last attempt to try and detect hydroxide groups in the samples was performed, which can be found in Figure 3.16. The measurements were allowed to run for a full hour to be able to detect low amounts of OH-groups and focused only on the narrow region where peaks corresponding to OH-bonds are visible. To reduce the background noise from the substrate the thin films were deposited on cleaned silicon substrates. Both measurements on crystalline and oxidized $Mg_{2.4}NiH_4$-samples were performed.

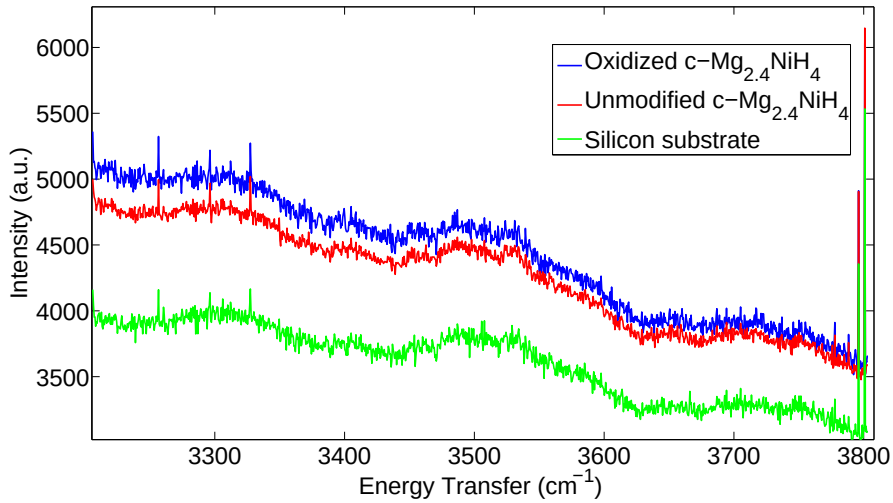

Figure 3.16: OH Region of the Raman spectra of $Mg_{2.4}NiH_4$-thin film deposited on silicon substrate.

In Figure 3.16 no difference can be seen between the clean silicon substrate and the thin films which would indicate the presence of hydroxide groups.

4 Discussion

Let's start the discussion with the result from the sample depositions. All samples have a uniform and similar color as deposited, independent of magnesium content. However upon heating, the samples with excess magnesium content, $Mg_{2.2}NiH_4$ and $Mg_{2.4}NiH_4$, first turn orange at 220C. Before 220C no color change is seen. There is little difference in this orange color between the samples, yet no crystallization has occurred because the XRD data reveals that the samples are still amorphous. So what is the reason for this color change? One explanation could lie in the size of the nanocrystals; upon heating the nanocrystals could grow in size, thus increasing the transmission. However that should be visible in the Raman spectra, which is not the case in the results presented in this thesis and just a change in crystallite size shouldn't change the magnitude of the band gap. The second explanation is that upon heating the crystal structure in some of the crystallites change from monoclinic to cubic, so the orange film consists of a mix of monoclinic and cubic crystallites. This should explain why the band gap of the orange films lies between the as deposited and crystallized samples. However to investigate this further TEM-measurements are suggested.

To achieve crystallisation of the thin films the temperature was increased to 290C. At this temperature the $Mg_{2.2}NiH_4$ and $Mg_{2.4}NiH_4$ samples change permanently to the same bright yellow color. So what happened to the $Mg_{2.0}NiH_4$ during annealing? Well not much, the samples might have turned slightly more transparent but the change is very subtle. However when synthesizing Mg_2NiH_4 nanoparticles excess of magnesium is standard practice, so this behavior is not unexpected.
The XRD-pattern for the yellow samples fits well with the reference pattern from nanoparticles with the cubic Mg_2NiH_4 structure. However there are some discrepancies, most notable is the peak at 19 degrees which is absent in the reference pattern. There are also slight shifts in the location of the other peaks compared to the reference data and when compared to each other, which could indicate that the dimensions of the unit cells might differ slightly between the samples and the reference.

To sum up the deposition of the thin films we can conclude that uniform samples were successfully synthesized. Upon heating, the samples with excess magnesium first turned into an amorphous, orange phase at 220C and at 290C the same samples crystallized. The $Mg_{2.0}NiH_4$ sample didn't change significantly upon heating.

One interesting phenomenon that was discovered in the annealing process was that some samples changed color when heated. The crystalline samples are yellow in room temperature while at higher temperature they gradually turned to a darker red color. This color change was seen as a decrease in the transmission spectra, while the reflection spectra only changed marginally, leading to a narrowing of the band gap. This thermochromic effect has not previously been found

in litterature for Mg_2NiH_4.

Narrowing of the band gap is seen in silicon as well at higher temperatures, only in the magnitude of a couple of meV [14]. So what could lie behind this big change? To investigate if this could be due to a structure change XRD measurements were done on a heated sample and compared to the result at room temperature. In the diffraction pattern from the heated sample the most striking difference is a broad peak at 17 degrees, however the nature of this peak was hard to identify. The remaining peaks were only slightly shifted and cannot explain the big change. Unfortunately there was a considerable background from the sample holder, which coincided with the peaks from the samples, so the intensities of the peaks could not be investigated.
Are there any other mechanisms that could explain the thermochromic effect? It could be linked to desorption of hydrogen, however the effect is reversible so it does not seem probable. Instead this could be due to changes in the material which are not detectable with XRD. The position of hydrogen in the material cannot be investigated directly with XRD so it is possible that the hydrogen atoms changes position upon heating which might lead to a change in the Mg-H interaction which is crucial to the band gap. To investigate this further it would be interesting to use a hydrogen sensitive technique to investigate the shape of the NiH_4 complexes, also temperature dependent Raman measurement would be interesting because if the shape of the Ni-H bonds affects the band gap this would be seen in the Raman spectra. Not only heating is interesting, spectrophotometry measurements on cooled samples would be of interest to see if the band gap changes.

Moving on to the electrical measurements conducted in the thesis, the $Mg_{2.4}NiH_4$ samples shows very high resistivities, matching that of intrinsic silicon, while the as deposited $Mg_{2.0}NiH_4$ has a significantly lower resistivity, which then is drastically increased upon heating.

These results differs significantly from the results obtained by Enache et al, they describe $Mg_{2.0}NiH_4$ as a heavily doped semiconductor with low electrical resistivity in the range of 0.1 ohm*cm. What could be the reason behind this big difference? First of all one must consider that their samples were slightly different with a palladium capping layer to prevent oxidizing the sample and to enable hydrogen loading after deposition. It is not impossible that this capping layer could affect the electrical properties of the material. They also detect large amounts of oxygen present in their sample but this does not seem to affect conductivity. Could the reason behind these relatively high resistivities also explain the strange behavior of the Hall-measurements and inability to determine the sign of several important properties? During the course of this thesis several attempts were done with different Hall-devices to try and measure important physical properties such as mobility and majority charge carriers of the material which would give vital knowledge about the material. Such experiments have been performed before in the previously mentioned paper by Enache [4], where Mg_2NiH_4 thin films were investigated with reasonable results.

So what could be the reason behind the high resistivities in the $Mg_{2.4}NiH_4$ samples? The first thing to discuss is the extra 20% magnesium atoms that do not fit into the crystal structure they can't disappear and must be ordered in the structure some way. A sign of this could be the

unidentified peak at 19 degrees in the GIXRD diffraction patterns. This could peak be assigned to metallic magnesium nanoparticles or other magnesium compounds present in the samples. However more peaks should be present if there were a substantial amount of foreign substances in the samples. It is also worth noting that the peak at 19 degrees disappears in the XRD pattern, which could indicate that this peak is related to a more long ranging structure since the planes of higher indices also 'disappear' in the XRD pattern. However both metallic magnesium nanoparticles and unwanted magnesium compounds would probably increase the resistivities in the samples.

To discuss the other peaks in the GIXRD pattern, one can notice that they are shifted slightly compared to the literature data. This difference could indicate that the unit cell in the thin film didn't have exactly the same side length as in the powder form, which would indicate that there might be some kind of strain in the thin films. Also there are some small differences in the diffraction patterns from $Mg_{2.2}NiH_4$ and $Mg_{2.4}NiH_4$ which indicates that the change in unit cell parameter is depending on the amount of extra magnesium added in the process.

The resistivity measurements on the $Mg_{2.0}NiH_4$ samples does indicate that the extra magnesium atoms actually increases the resistivity in the samples. The as deposited sample has a resistivity that is much lower that that of the as deposited $Mg_{2.4}NiH_4$ samples which indicates that the scattering defects in the sample is much lower with lower magnesium content. However the resistivity are still a factor 10^3 higher than in previous results. Since the $Mg_{2.0}NiH_4$ samples were amorphous no XRD-pattern could be recorded for these samples. The results from the annealed $Mg_{2.0}NiH_4$ samples must also be mentioned, the low resistivity only applies for the as deposited samples, when annealed the resistivity increases drastically. The reason why this occurs could be due to a change in crystallite size upon heating, which should be seen in the Raman spectra as sharpening of the peaks which is demonstrated in Raman spectra on silicon samples with different crystallite sizes [8]. Another possibility is that oxides are formed on the surface, creating an insulating layer, but no peaks from such a layer could be detected which might indicate that it's very thin.

To sum up the discussion so far about the connection between the Hall-measurements, resistivity measurements, XRD-result and impurities there is a big difference in resistivity between the as deposited $Mg_{2.4}NiH_4$ and $Mg_{2.0}NiH_4$ samples, which could be explained by the presence of extra magnesium atoms. Still however the resitivities are much higher than expected from previous papers even with the correct amount of magnesium. Could these magnesium atoms also explain the strange Hall-measurements? Maybe, if the number of charge carriers is too small and the scattering defects are too many then they will be recombined very quickly, thus reducing the amount of charge carriers and the current, making the Hall-current too weak to be measured. Hall-measurements were performed on $Mg_{2.0}NiH_4$ samples as well with the same result as $Mg_{2.4}NiH_4$, so this indicate that there are other impurities in the material as well.

It could also be that there are impurities in the sample that originate from the deposition which affects the conductivity without acting as a dopant. For example a small portion of air is still

in the load lock when the carrier is transferred from the load lock to the processing chamber. Consequently oxygen, carbon dioxide and other residual gases are most probably present in the processing chamber during the deposition and will be incorporated into the films and bind with the nickel or magnesium atoms thus affecting the structure and physical properties of the material. During the autumn, experiments with Rutherford Backscattering Spectrometry (RBS) measurements were performed to try and measure the amount of impurities in the deposited films. The result showed that carbon was present to a large extent in the samples and thus can be assumed to affect the conductivity properties. These data will be presented later in a paper by Raskovic-Lovre.

Another possible explanation of the presence of impurities in the sample could lie in the targets used in the sputtering process. The purity and composition of these were discussed previously in the thesis, it could be so that there are impurities such as silicon, carbon and other metal atoms which are sputtered from the targets which also affects the compositions. A quick EDS measurement was performed on the 'Mg_2Ni'-target and the small splinter that was analyzed showed that the composition is only '$Mg_{1.55}Ni$' and that other unwanted atomic species also was present in the target.

To summarize the discussion regarding the properties of the sputtering device, one could say that the sputtering device used in this thesis was a black box, with many unknown parameters which affects the composition of the deposited samples. It might not seem important if a few oxygen atoms go into the samples or not, but when discussing impurities in semiconductors it is important to keep in mind that a very small amount could drastically change the conduction properties. In silicon wafers for solar cell production a purity of 99.9999% is required for solar cell grade silicon. For the magnesium and 'Mg_2Ni'-targets the purity is only guaranteed to 99.99% which together with the presence of unwanted gases in the processing chamber might indicate that the purities of the synthesized films are too low to be suitable for semiconductor production.

To identify the presence of impurities in the films, but also to investigate the bonding present in the material, Raman spectroscopy measurements were conducted on all samples. To start with the spectra from the amorphous materials, they differ significantly from the literature spectra and also from the spectra from the crystalline samples. All of the spectra from the different amorphous samples look very similar, no clear change is visible which would indicate a change in the crystallite size. However there are two significant features that need to be discussed. The first feature is the very sharp peak at 182 cm^{-1} which is not present in the literature and is very sharp. It was first assigned to the Mg-translation peak, but the sharpness of the peak led to a discussion of its origin, and after investigating different possibilities it was concluded to most probably be a plasma line artifact from the HeNe-laser. As such this peak does not belong to the sample itself but to the laser, so it has been excluded from any further discussions. The second interesting feature, or maybe more a lack of feature is the absence of the Ni-H bond peaks. This was very surprising and could first not be explained by other than that the NiH_4-complexes maybe wasn't present in the material. But after discussing the question with the technician specialized in Ra-

man spectroscopy at the department the issue of the magnitude of the band gap came into light. The amorphous samples have band gaps between 1.53eV to 1.85eV which is less than the laser energy at 1.96eV. When the band gap is narrower than the laser this might lead to certain effects in the Raman spectra, due to the fact that the laser can excite electrons across the band gap. This is most probably the reason why the Ni-H is missing.

On the other hand, Raman spectra from the crystalline $Mg_{2.4}NiH_4$ and $Mg_{2.2}NiH_4$ samples are very similar and both are more or less consistent with the literature data. However there are still deviations and peak assignment is difficult in the low energy region, while the Ni-H peaks appear as expected. The band gap of the crystalline samples is in the region of 2.04eV to 2.15eV so the laser is unable to excite the electrons and the laser energy is very close to the excitation energy. These are conditions that leads to a so called Resonant Raman mode, where a strong enhancement of the Raman signals occurs. The theory behind this phenomenon can be found in the book 'Semiconductor Physics' [7].

Since no clear peaks from oxides or other contaminations were detected in the Raman spectra of the deposited samples, two samples were exposed to distilled water to force the films to oxidize. During the process, small gas bubbles formed on the surface and a film seemed to be formed at the surface, which changed the color of the film slightly. Then Raman spectra were obtained for both samples and they showed that in the crystalline sample the Ni-H peaks disappeared and in the sample from the amorphous sample exposed to water there was a new peak present at 550 cm^{-1}. This could be a sign that when the films are oxidized in water the NiH_4 complexes changes into NiO, however more investigations should be done before any conclusions can be made.

To summarize the results from the Raman measurements, the spectra of the amorphous materials show little resemblance with the previous measurements found in the literature. Most notably is the lack of peaks for the Ni-H bond, which would indicate that these bonds are missing in the material. However the relationship between the energy of the laser and the band gap plays an important role possibly enhancing the Raman signals, which in the case of the amorphous materials might lead to the fact that the Ni-H peaks are too weak. No presence of oxide bonds or other unwanted contaminations can be assured in any of the samples, this might be due to very small amount or that some of the impurities simply aren't Raman active. As for the increase of resistivity in the $Mg_{2.0}NiH_4$ samples; if it was due to a change in crystallite size, this should be seen in the Raman spectra if $Mg_{2.0}NiH_4$ interacts the same way as silicon.

The last thing that will be discussed is the difference in band gap between the different compositions and structures, which is most striking in the $Mg_{2.2}NiH_4$ and $Mg_{2.4}NiH_4$ samples. This change in bad gap simply by going from amorphous, or nanocrystalline, to crystalline is not seen in other materials such as silicon. In silicon there is only a subtle change in the band gap between amorphous, nanocrystalline, microcrystalline and crystalline structures. So why is the change so big in this case? The answer probably lies in the fact that inside the crystallites in the amorphous samples the monoclinic structure is present. The monoclinic structure has a different band structure, and band gap compared to the cubic structure.

5 Conclusions and outlook

Now it is time to draw some conclusions based on the results in this thesis and to answer the questions stated in the introduction. Let's start with the deposition of the thin films, where three different compositions were synthesized: $Mg_{2.4}NiH_4$, $Mg_{2.2}NiH_4$ and $Mg_{2.0}NiH_4$. The compositions were determined by EDS and showed to be quite uniform with small compositional variations. Two thin films with the composition $Mg_{2.4}NiH_4$ and $Mg_{2.2}NiH_4$ were successfully annealed and crystallized irreversibly to a monocrystalline cubic structure at 290C which confirms the results from previous work on Mg_xNiH_4 gradients. An intermediate orange state was also found when the $Mg_{2.4}NiH_4$ and $Mg_{2.2}NiH_4$ samples were heated to 220C, this state was found to be amorphous from XRD-measurements and is not described previously in the literature. However XRD-measurement showed no signs of structure change in the $Mg_{2.0}NiH_4$ samples which confirms that an excess of magnesium atoms are required to achieve the crystalline structure.

The second question was regarding the presence of impurities and defects in the thin films, which were investigated with XRD and Raman spectroscopy. And we can conclude that no impurities in the form of hydroxides, MgO or NiO were found in the Raman spectras, but since not all peaks were identified to 100% it could be possible that other impurities such as metallic clusters or foreign atomic species could be present, but not identified in the spectra, so more research is required. However Raman measurements om thin films immersed in distilled water showed signs of being oxidized and possibly forming NiO, but again more research such as XRD-measurements on the oxidized films would be interesting. The results from the XRD measurements performed on the crystalline $Mg_{2.4}NiH_4$ and $Mg_{2.2}NiH_4$ samples was quite consistent with literature data, and the small change in the position of the peaks could be explained by a small change in the dimensions of the unit cell, which could indicate that there are some strain present in the material. The most important difference between the reference and the obtained data is a peak at 19 degrees which is present in our samples but not in the reference. This peak could be assigned to foreign compounds such as oxides present in the material, or structural defects. However more peaks should be present if there is another crystal structure mixed with the cubic Mg_2NiH_4 structure. The peak also showed that it had some long ranging characteristics because it was not present in the XRD-data from measurements taken with a bigger incidence angle.

The final question on the structure is how the hydrogen atoms are distributed in the material. Raman spectroscopy was used once again to investigate the presence of different bonds in the material. Ni-H bonds were detected in the two crystalline samples, but it is hard to say if the bonds change somehow with different magnesium content. However no Ni-H bonds were detected in the amorphous materials, and these Raman spectra differed significantly from the reference spectra. This was a quite unexpected result and can probably be explained by the relationship between the laser used and the magnitude of the band gap, where the band gap is smaller than the laser in the amorphous materials. But most likely they are bonded in a similar way as in

the crystalline samples, however to confirm this a Raman measurements with weaker laser is required.

The next step was to investigate the physical properties, firstly the band gap of the different samples were calculated using transmission and reflection spectra from spectrophotometry. The result showed that the as deposited samples for all compositions had quite similar band gap with a slightly smaller band gap for the $Mg_{2.0}NiH_4$ sample. The band gap for the $Mg_{2.0}NiH_4$ sample were also almost unaffected by heating. That cannot be said about the $Mg_{2.4}NiH_4$ and $Mg_{2.2}NiH_4$ samples, upon annealing the band gap increased both in the samples annealed at 220C and 290C where the band gap of the orange samples were in between the as deposited samples and the crystalline samples. The band gap of the as deposited and crystallized samples is consistent with previous measurements. The big change in the band gap between the annealed $Mg_{2.2}NiH_4$ and $Mg_{2.4}NiH_4$ samples is probably explained by a change in the crystal structure from a monoclinic structure inside the crystallites in the as deposited structure to the cubic structure in the annealed samples.

What conclusions can be made regarding the resistivity to magnesium content and annealing process and how does it compare to previous measurements? The $Mg_{2.0}NiH_4$ and $Mg_{2.4}NiH_4$ samples showed very different characteristics, the $Mg_{2.0}NiH_4$ sample measured a very low resistivity in the as deposited state which increased drastically upon heating and the highest resistivity measured was found in the $Mg_{2.0}NiH_4$ sample annealed at 290C. For the $Mg_{2.4}NiH_4$ sample the resistivity hardly changed upon annealing. The big change in resistivity for the $Mg_{2.0}NiH_4$ sample could be explained by a change in size of the crystallites, however this should be seen in the Raman as broadening of the peaks but no such change is seen. Compared to previous data the resistivities are very high in all cases compared to both capped films investigated previously [4] and measurements done on uncapped gradients [13].

The Hall-measurements that were conducted in the thesis gave some contradicting and interesting results, essentially the Hall-current seems to be to weak to measure by the devices we used making it impossible to determine the sign of the charge carrier mobility and density. This is contradicting previous Hall-measurements conducted on Pd-capped thin films, which describes the $Mg_{2.0}NiH_4$ as a heavily doped semiconductor.

During the annealing process of the samples we noticed that the crystalline $Mg_{2.2}NiH_4$ and $Mg_{2.4}NiH_4$ samples changed to a dark red color upon heating. This thermochromic effect was investigated with spectrophotometry and XRD analysis, the conclusions that can be made are that the change is reversible and that the band gap is decreased with almost 0.3eV when heated to 300C. The structure of the heated sample was measured with XRD to see if any change occurs, unfortunately there is a background signal from the sample holder which interferes with the peaks from the sample. However a broad peak appears at 17 degrees which cannot be identified and is not present in other measurements. The shape of the peak itself is quite broad and it is hard to say what could be the reason behind this peak, another attempt with a different setup would be interesting both to investigate the unidentified peak and to avoid the peaks from the

sample holder. Hydrogen desorption was also ruled out to be the reason behind the color change since it is reversible. So the color change is probably due to a change in the positions of the hydrogen atoms, it would be interesting to investigate this further using neutron scattering on heated samples.

Which conclusions can be made on the relationship between resistivity and structure results? The Raman spectra result do not give any indication on the presence of any impurities in the form of oxides or hydroxides, when it comes to metallic clusters or other impurities it is difficult to draw any conclusions due to the fact that some of the peaks were shifted when compared to the reference data. The peak at 19 degrees in the XRD results indicates that something unidentified is present in the structure, which would lead to an increase in resistivity either if it is from impurities or defects in the thin films. It is also most likely that the targets used in the deposition process have to low purity to successfully deposit semiconducting thin films and substitution defects could be fatal to the transport process and physical properties of the charge carriers without being detectable in Raman or XRD.

What is the outlook of the future research regarding Mg_2NiH_4? From this thesis one might say that the possibility of introducing Mg_2NiH_4 as a new semiconductor material in the solar cell industry is rather slim. However before ruling it out completely I would say that some issues need to be further investigated. First of all a the impurities in the material needs to be more thoroughly investigated, I would suggest that methods such as EXAFS and XPS should be used to see what unwanted atomic species are present in the material. Also I would suggest that a residual gas analyzer should be invested in for the sputtering system to actually now what is left in the chamber during the depositions. To detect structural defects further TEM measurements would be interesting. I also think it would be interesting to investigate the semiconducting properties of Mg_2NiH_4 in the form of nanoparticles as a component in so called hybrid solar cells. For better understanding of which role hydrogen plays in the material I would like to see neutron scattering experiments to be performed on samples in the form of thin films, both crystalline and amorphous. But also techniques such as FTIR and FT-Raman would be interesting to investigate the nature of the Ni-H bonds and how the structure of the material affects them.

The last part that would be interesting to investigate is the thermochromic effect seen in the $Mg_{2.4}NiH_4$ material. In this case I would like to redo the temperature dependent XRD measurements, but also measure the transmission and reflection spectra of $Mg_{2.4}NiH_4$ samples at lower temperatures. Temperature dependent Raman and spectrophotometry measurements would also be interesting to see what happens when the sample is cooled down or heated up.

References

[1] Emanuele Centurioni. Generalized matrix method for calculation of internal light energy flux in mixed coherent and incoherent multilayers. *Appl. Opt.*, 44(35):7532–7539, Dec 2005.

[2] D. M. Chapin, C. S. Fuller, and G. L. Pearson. A new silicon p-n junction photocell for converting solar radiation into electrical power. *Journal of Applied Physics*, 25(5):676–677, 1954.

[3] Thomas Dieing. *Confocal Raman Microscopy*. Springer, 1 edition, 2011.

[4] S. Enache, W. Lohstroh, and R. Griessen. Temperature dependence of magnetoresistance and Hall effect in Mg_2NiH_x films. *Phys. Rev. B*, 69:115326, Mar 2004.

[5] G. N. García, J. P. Abriata, and J. O. Sofo. Calculation of the electronic and structural properties of cubic Mg_2NiH_4. *Phys. Rev. B*, 59:11746–11754, May 1999.

[6] Michèle Gupta. The electronic structure of hydrogenated intermetallic compounds: Theory. *Journal of the Less Common Metals*, 101(0):35 – 51, 1984.

[7] Jordi Ibáñez and Ramon Cuscó. Raman spectroscopy of compound semiconductors. In Amalia Patane and Naci Balkan, editors, *Semiconductor Research*, volume 150 of *Springer Series in Materials Science*, pages 259–281. Springer Berlin Heidelberg, 2012.

[8] Z Iqbal and S Veprek. Raman scattering from hydrogenated microcrystalline and amorphous silicon. *Journal of Physics C: Solid State Physics*, 15(2):377, 1982.

[9] S. Zh. Karazhanov and A. G. Ulyashin. Similarity of electronic structure and optical properties of Mg_2NiH_4 and Si. *EPL (Europhysics Letters)*, 82(4):48004, 2008.

[10] S.Zh. Karazhanov, A.G. Ulyashin, P. Vajeeston, and P. Ravindran. Hydrides as materials for semiconductor electronics. *Philosophical Magazine*, 88(16):2461–2476, 2008.

[11] Charles Kittel. *Introduction to Solid State Physics*. John Wiley & Sons, 7 edition, 1996.

[12] R. Martinez-Coronado, M. Retuerto, and J.A. Alonso. Simplified mechano-synthesis procedure of Mg_2NiH_4. *International Journal of Hydrogen Energy*, 37(5):4188 – 4193, 2012.

[13] T. Mongstad, C.C. You, A. Thogersen, J.P. Maehlen, Ch. Platzer-Björkman, B.C. Hauback, and S. Zh. Karazhanov. $Mg_yNi_{1-y}H_x$ thin films deposited by magnetron co-sputtering. *Journal of Alloys and Compounds*, 527(0):76 – 83, 2012.

[14] K. P. ODonnell and X. Chen. Temperature dependence of semiconductor band gaps. *Applied Physics Letters*, 58(25):2924 –2926, jun 1991.

[15] OECD. Electricity generation.

[16] Stewart F. Parker, Kenneth P. J. Williams, Tim Smith, Manfred Bortz, Bernard Bertheville, and Klaus Yvon. Vibrational spectroscopy of tetrahedral ternary metal hydrides: Mg_2NiH_4 Rb_3ZnH_5 and their deuterides. *Phys. Chem. Chem. Phys.*, 4:1732–1737, 2002.

[17] T. J. Richardson, J. L. Slack, R. D. Armitage, R. Kostecki, B. Farangis, and M. D. Rubin. Switchable mirrors based on nickel–magnesium films. *Applied Physics Letters*, 78(20):3047–3049, 2001.

[18] Trygve Tveiterås Mongstad. *Thin-film metal hydrides for solar energy applications*. PhD thesis, University Of Oslo, 2012.

[19] J.H. Selj, T. Mongstad, B.C. Hauback, and S.Zh. Karazhanov. The dielectric functions and optical band gaps of thin films of amorphous and cubic crystalline $Mg_{\sim 2}NiH_{\sim 4}$. *Thin Solid Films*, 520(22):6786 – 6792, 2012.

[20] William Shockley and Hans J. Queisser. Detailed balance limit of efficiency of p-n junction solar cells. *Journal of Applied Physics*, 32(3):510–519, 1961.

[21] Wikipedia. Band structure, 2012. [Online; accessed 29-November-2012].

[22] Wikipedia. Energy-dispersive x-ray spectroscopy, 2012. [Online; accessed 12-December-2012].

[23] Wikipedia. Pn junction diffusion and drift, 2012. [Online; accessed 28-November-2012].

[24] Wikipedia. Raman spectroscopy, 2012. [Online; accessed 1-November-2012].

[25] Wikipedia. Sunlight, 2012. [Online; accessed 13-December-2012].

[26] Wikipedia. Hall effect, 2013. [Online; accessed 13-January-2013].

[27] Wikipedia. Solar cell, 2013. [Online; accessed 14-January-2013].

[28] B. G. Yacobi and ebrary (e-book collection). *Semiconductor materials: an introduction to basic principles*. Kluwer Academic Publishers, New York, 2003.

[29] K. Yvon, J. Schefer, and F. Stucki. Structural studies of the hydrogen storage material Mg_2NiH_4.